Neural Activity in Primary Motor Cortex: a System Level Physiological Model

Ehud Trainin[1], Ron Meir[1], Amir Karniel[2]

[1] Department of Electrical Engineering, Technion, Haifa, Israel

[2] Department of Biomedical Engineering, Ben-Gurion University, Beer-Sheva, Israel

Correspondence should be addressed to rmeir@ee.technion.ac.il

Abstract

What determines the specific pattern of activation of primary motor cortex (M1) neurons in the context of a given motor task? In order to address this question, we develop a system level physiological model and compare its predictions with experimental data related to the caudal part of M1, during voluntary trained tasks. Our model describes the transformation from the neural activity in M1, through the motor control signal, into joint torques and down to endpoint force and movement. The redundancy of the system is resolved by adding a biologically plausible optimization criterion. We compare the predictions of our model to the experimental results and reproduce the observed activity in M1 during a variety of tasks. Using our model we were able to explain, for the first time, many basic experimental observations in a mechanistically explicit way.

1

Introduction

The primate motor system is a highly complex system leading to sophisticated motor activities resulting from the concerted activity of multiple cortical, sub-cortical and skeletal modules involving multiple feedback loops[1] [1]. In this work we focus on simple tasks for which a system level physiological model is provided. Specifically, we focus on the primary motor cortex (M1), which plays a major role in voluntary limb movement. Projections from M1 influence muscles through direct synapses on motor-neurons and indirectly through spinal inter-neurons [2]. Each M1 neuron affects several muscles, while each muscle is in turn affected by many M1 neurons. One problem in explaining neural activity in M1 results from the confusing experimental findings related to the level of abstraction of M1 control signals. This is a much debated and controversial issue [3] with significant implications on prosthetic neuro-controllers [4]. In fact, M1 is highly heterogeneous [5,6,7,8], as different regions in M1 represent different levels of motor control output, and therefore cannot be uniformly interpreted. Even so, explaining neural activity within a *specific* region of M1 is challenging, as the controlled system is highly redundant [9], implying that a given task may be accomplished by many possible control signals. In order to understand why M1 produces a *specific* control signal, some means needs to be introduced for allowing the system to select a single control command. The main question addressed in this paper is what determines the specific pattern of activation of M1 neurons in the context of a given motor task? Using the mathematical framework of optimal control theory, we formulate this question as follows: What are the neural and the biomechanical *constraints* imposed by the system, and what are the internal goals of the brain (specified by an objective function), according which it selects a specific control signal, given the huge redundancy in the system?

We proceed with a more detailed description of the above issues and the differences between our approach and previous work. A temporal tuning function is usually defined as a function that maps time-dependent external force or movement direction into temporal neuronal firing rates. A standard way of analyzing M1 experiments is based on fitting firing rates to a cosine-tuning function [10], calculating the preferred direction (PD) of each neuron (the direction corresponding to the peak of the tuning function) and forming the population vector, defined as the sum of neuronal firing rates (relative to each cell baseline) multiplied by their PD unit vector [11]. The population vector was found to be a reasonably accurate estimator of hand movement or force direction [12,13,14]. One possible interpretation of cosine tuning and of the population vector is that M1 employs a coding scheme based on external space directions. This interpretation is known as *direction coding*. While the pioneering experiments [10,11] might give the impression that direction coding is a simple key to M1 neural activity, many subsequent experiments demonstrated that the picture is far more complex [15]. In fact, neurons in M1 do not possess a single fixed PD. Rather, the PD depends on external variables (such as force or velocity) with which the neuron is correlated. The correlations change for different tasks, and also as a function of time within a *single* task. Moreover, the neural activity of many motor cortical cells is not determined solely by the spatial attributes of the hand trajectory [16,17,18]. Furthermore, some experimental findings have demonstrated a close relationship between M1 neural activity and EMG [19,]

[20, 21]. The question then is whether cells in M1 control high-level movement features, such as the direction of hand movement, or whether they control specific pattern of muscles activity? Another controversial and closely related question is whether M1 employs equilibrium point control [22]. According to the equilibrium point hypothesis, the muscles and the spinal cord compensate for the arm's dynamic or, at least, to part of it. Consequently, the movement control task of the CNS is more abstract.

Needless to say, an understanding the level of abstraction used by M1 is still lacking. In fact, a gradation of possibilities exists between high-level control and direct muscle control. Furthermore, the translation from temporal patterns in external space into dynamic patterns in muscle space does not take place in a single isolated area. As noted above, M1 neural activity is heterogeneous as multiple levels of motor output representation are distributed across M1 [8]. However, using a low level muscle control model we were able to explain neural activity in M1. The experimental results we've examined [8,19,20,23] are related to the caudal part of M1, during voluntary trained tasks. Therefore, while our results are consistent with the low level control hypothesis, they are not in contradiction with the evidence for higher levels of computation in M1.

Our system level physiological model describes the transformation from the neural activity in M1, through the muscle control signal (MCS), into joint torques and down to endpoint forces and movements. The redundancy of the system is resolved by adding a biologically plausible optimization criterion related to energy consumption. Each trajectory in the space of neural inputs to the muscles is associated with a cost value, and the selected trajectory is the one for which the cost is minimal.
Our model aims at being the simplest physiological model able to predict the complex patterns of M1 neural activity. Despite its relative simplicity, it appears to capture key features of the spinal cord and the biomechanical system in the context of the tasks studied. We compare the predictions of our model to experimental results [8,19,20,23] and reproduce the observed activity in M1. The model's predictions provide a surprisingly good approximation to a variety of non-trivial experimental results that, to the best of our knowledge, have not been previously explained in a mechanistically explicit model. We aim at providing predictions of neural activity at the level of a population rather than at the level of single cells. However, as we demonstrate, we are able to explain a variety of phenomena at the level of single neurons. This seeming contradiction is explained as follows. First, the population activity constrains the possible patterns of activity of single cells. Second, the experimental results we have examined [8,19,20,23] display a considerable amount of similarity between population activity and single cell activity. The diversity of cell responses and their dependence on the specific task can, to a large extent, be accounted for by properties of the control signals; we elaborate on this issue in the Results. Nevertheless, not all the diversity of neuronal behaviors can be accounted for by the control signal properties. This issue is left open for future research.

Since the bio-mechanically controlled system is a dynamical system, a time instance of a low level control signal is meaningful only within the context of its complete task. Therefore, in our view the

temporal tuning functions merely provide an analysis tool, lacking any intrinsic biological meaning. In particular, in our study we show that (i) The tuning function is not always cosine-shaped, and (ii) Cosine behavior does not suffice to characterize the tuning function, as further properties of the tuning function have an informative value, such as the support of the tuning function, i.e., the domain over which the function value differs from zero. In fact, the PD is not a basic invariant characteristic of the neuron. In particular, our model explains changes in the PD between tasks and during a single task. Instead of the PD, the neuron is characterized in our model by its relationship to the MCS. The population vector also possesses no intrinsic biological meaning; rather it merely provides an algorithm for movement prediction. In particular, our model explains the observed deviations of the population vector from the force direction. Instead of a population vector in external space coordinates, MCSs describe population behavior in our model. We emphasize again that the above view of neural coding in caudal M1 is not in contradiction with views of high level coding, since the motor cortex is highly heterogeneous.

The idea that correlations with high level parameters may (sometimes) be an outcome of low level representation is known as the *muscle-coding hypothesis* [24]. While our model was inspired by muscle-coding hypothesis [24], it differs in focus and detail. The muscle coding hypothesis was not intended to constitute a physiological model and indeed one cannot interpret it in such a way. In particular, the muscle coding hypothesis does not determine the identity of the muscle-related variables encoded by neurons in M1 (the variable of planned muscle shortening velocity was given only as an example [24]). Nor does it specify the physiological elements and the mechanisms involved in executing this muscle plan. Finally, the muscle coding hypothesis explained the same phenomena addressed by the direction coding hypothesis, i.e., cosine tuning and the population vector. Therefore, the question as to whether M1 neurons control specific patterns of muscle activation remained unresolved. As we show in this study, there are many phenomena related to neural activity in M1, which can be explained solely by the similarity between M1 neural activity and muscle activity.

As far as we are aware, there has been only a single attempt to develop a system level physiological model that explains M1 neural activity during voluntary movement [25,26]; we refer to this model as TOD2000. This model is very different from ours both in its concept, as well as in the predicted results. Essentially, TOD2000 is based on non-physiological assumptions - see detailed discussion in Supplementary Data 2, as well as the criticism raised in [27,28]. In fact, TOD2000 is a certain type of direction coding model and therefore suffers from all the inherent limitations of such models, such as an inability to explain changes in the PDs during a task [20], and between tasks [19] or deviations of the population vector from expected directions [8]. As we show in Results and Supplementary Data 2, our system level physiological model provides better predictions and interpretations of the experimental data.

Results

We consider three sets of experiments performed by Sergio and Kalaska[8,19,20,23], and present comparative model results for all cases. Recall that our main objective here is to 'reverse engineer' the neural control signal based on the optimization criterion proposed and on the biological constraints imposed. Our physiological model successfully predicts population neural activity in the caudal part of M1 during trained voluntary tasks. Furthermore, the results display considerable similarity between the muscle control signal and the neural activity of a single neuron. Based on this similarity, our model provides a qualitative explanation for a variety of phenomena at the level of the single cell as well. Our simulation uses several parameters taken from[29,30,31]. As in any modeling approach, one needs to address the sensitivity of the results to model parameters. As we show in Supplementary Data 6, our results are robust with respect to a wide range of parameter variations. In Fig. 1, 2, 4 and 5 we added the predictions according to TOD2000. We discuss these graphs (and all the other results) in detail in Supplementary Data 2, and compare our model with the predictions of TOD2000.

Isometric Task

In the first experiment[8,20] a monkey was trained to perform an isometric task, i.e. the monkey retained a fixed end-point position in the face of an external force field. The monkey was required to exert a ramp force in one of eight directions, spaced at 45° intervals. For a detailed description of the experimental setup see Supplementary Data 3.

Control Signal

A major prediction of our model pertains to the MCS. In Supplementary Data 3 we present the MCSs predicted by our model, as well as explanations of the derivation of these results. In order to calculate a MCS from of the experimental neuronal activity (see Equation (1) in Methods) we should estimate the weight and the latency of each neuron with respect to each of the MCSs. Unfortunately, without access to the full experimental data such a calculation is not feasible; however, the average response of 132 neurons aligned to their PD is available [8] as shown in Fig. 1a. Based on the control signals predicted from our model, we approximate the predicted averaged response as shown in Fig. 1b. In order to reduce the effects of the simple averaging procedure described in the legend of Fig. 1, we also compare the predicted control signal with a response of a *single* representative neuron for two force directions (Fig. 2). The good qualitative match between the experiment and model can be clearly observed in Fig. 1 and 2.

a

b
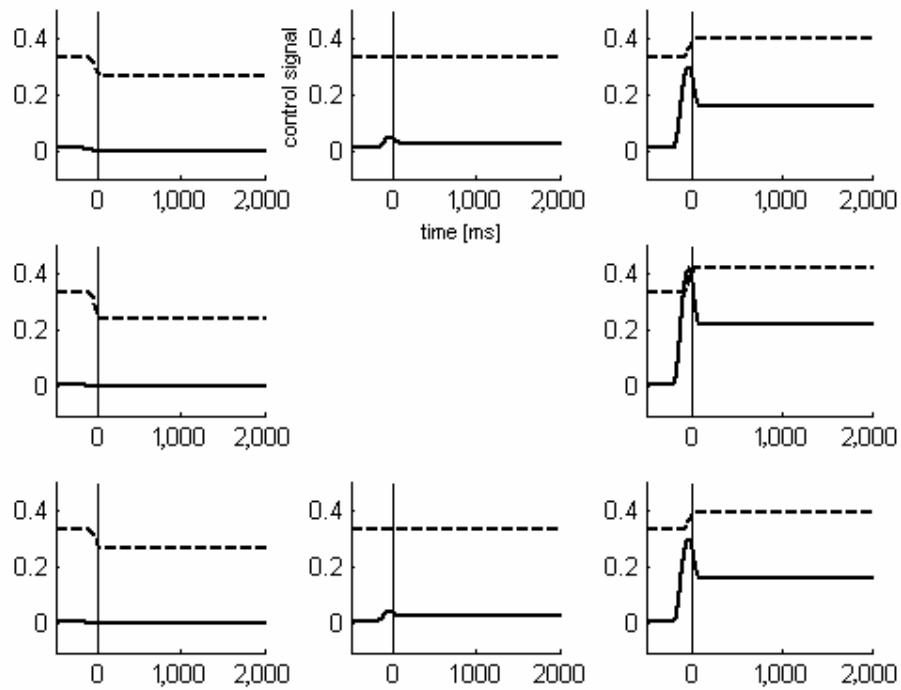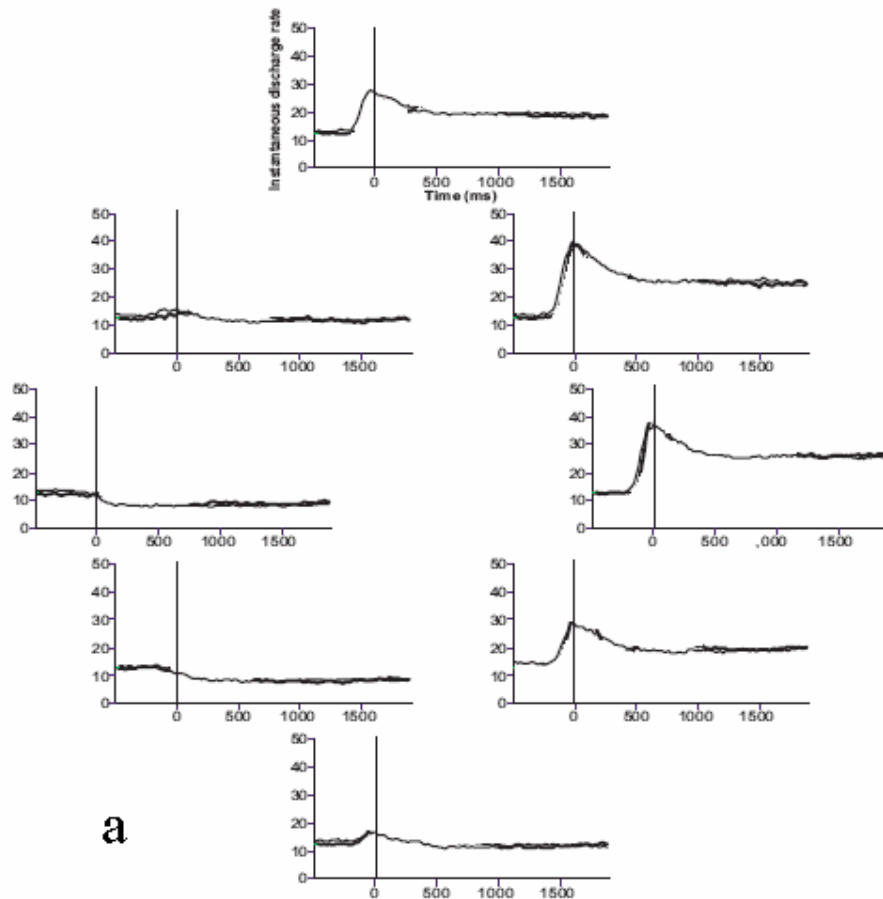
Figure 1: Population activity for the isometric task. **1a:** Experiment, based on Fig. 9 of [8] with permission. Mean population response as a function of time and force direction, where the direction is relative to the PD of each cell. All data were aligned to the time of force onset (time 0) and the PD of each neuron was arbitrarily rotated to the right. **1b:** Simulation of average neural response in our model (solid line) and the control signal of TOD2000 (dashed line). The baseline in TOD2000 is assumed to be 4. The control signal of TOD2000 was normalized by multiplication by 0.12, which is the maximal value preventing a negative control signal during the movement experiment at 180°. The ordinate of simulation of our control signal is normalized to arbitrary units. The simulation of the averaged neural response was performed using the following assumptions: **(1)** In creating the control signal in our model different neurons do not necessarily have the same weight. There are several reasons for this. A PD of a neuron may be different from the PD of the control signal. Moreover, different neurons possess different weights in the spinal cord summation mechanism. In creating Fig. 1b, we ignore these problems assuming that a simple average approximates the linear combination which produces the control signal in our model. **(2)** Different neurons possess different latencies. In order to compensate for this we've smoothed the predicted control in our model assuming that the profile of activity of all neurons is similar except for the latency; that the latency is distributed uniformly in the range of [50msec, 200msec]; and that the weights of all neurons in the control signal are equal. **(3)** In the calculation of the experimental averaged response, each neuron response was aligned to its PD, given within a resolution of 45°. This low resolution creates a smoothness effect in the direction axis as well. In order to compensate for this we've   smoothed the predicted control in our model assuming that the directionality alignment is distributed uniformly in the range of [-22.5°, 22.5°]; and that the weights of all neurons in the control signal are equal the same.
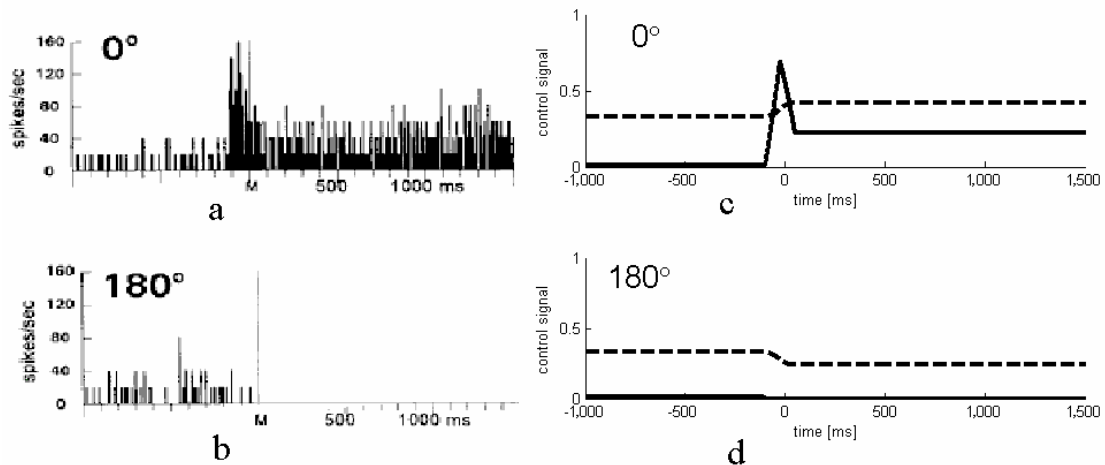
Figure 2: Isometric task – comparison with activity of a representative cell. **2a:** Experiment, based on Fig. 1a from [8], with permission. Discharge pattern at the PD of a shoulder-related M1 cell in histogram format (10-ms bins). Data are aligned on the first significant force change, denoted by a solid vertical line (M). **2b:** The same as 2a, in the opposite direction. **2c:** Simulation of Shoulder extensor control signal in our model (solid line) and the control of TOD2000 (dashed line) at the PD. The baseline and the normalization of the control signal of TOD200 are as in Fig. 1. We assume for both models that the control signal is delayed by 100msec. The ordinate of simulation of our control signal is normalized to arbitrary units. **2d:** The same as 3c, in the opposite direction.

Single cell properties

While the control signal resulting from our model agrees with the experimental results, we must keep in mind that neuronal responses are not identical. However, the diversity of cell activity as reported in [8,20] is not high. Out of 72 recorded cells in [20] 36% displayed a step response in their PD, 28% displayed pulse-step response, 29.3% displayed a pulse response and 6.7% were unclassifiable. Thus, three typical behaviors of cell activity as a function of time were observed, each of them similar to the computed control signal or to part of it. Thus, the behavior of the predicted control signal plays an important part in the explanation of single cell activity.

Cosine tuning

The predicted control signals are cosine tuned, where the support of each of the tuning functions in this experiment is approximately 180°. We refer to the Supplementary Data 3 for details of the derivation of these results. The experimentally reported cosine tuning at the level of the single cell provides an additional indication of the similarity between cell activity and the control signal activity.

Furthermore, the support of the control signal imposes a limitation on the support of the single neuron response. Therefore, we expect that the support of a single neuron should be about 180° or less. In particular, the tuning function of a neuron might be further narrowed if it influences more than a single joint, as analyzed in Supplementary Data 8. This prediction is in agreement with the experimental results [8,20] shown in Supplementary Data 8. However, we do not have data about the tuning function support of all cells; such data is needed in order to further test this prediction.

Muscle Directionality Amplification

How far is directionality preference at the level of a single cell similar to directionality preference at the level of the MCS? In the case of high similarity, we would expect that neurons with PD closer to the muscle PD will be more dominant. The dominance may be achieved in several ways, which cause a shift of the population vector towards the nearest amplified direction – see Supplementary Data 7. We will refer to this hypothesis as *muscle directionality amplification*. In the particular experiment we've examined, most neurons were related to the shoulder. Therefore, we expect that the population vector will be shifted towards the PDs of the shoulder flexor and the shoulder extensor. This prediction is in good agreement with the results shown in Fig. 3.
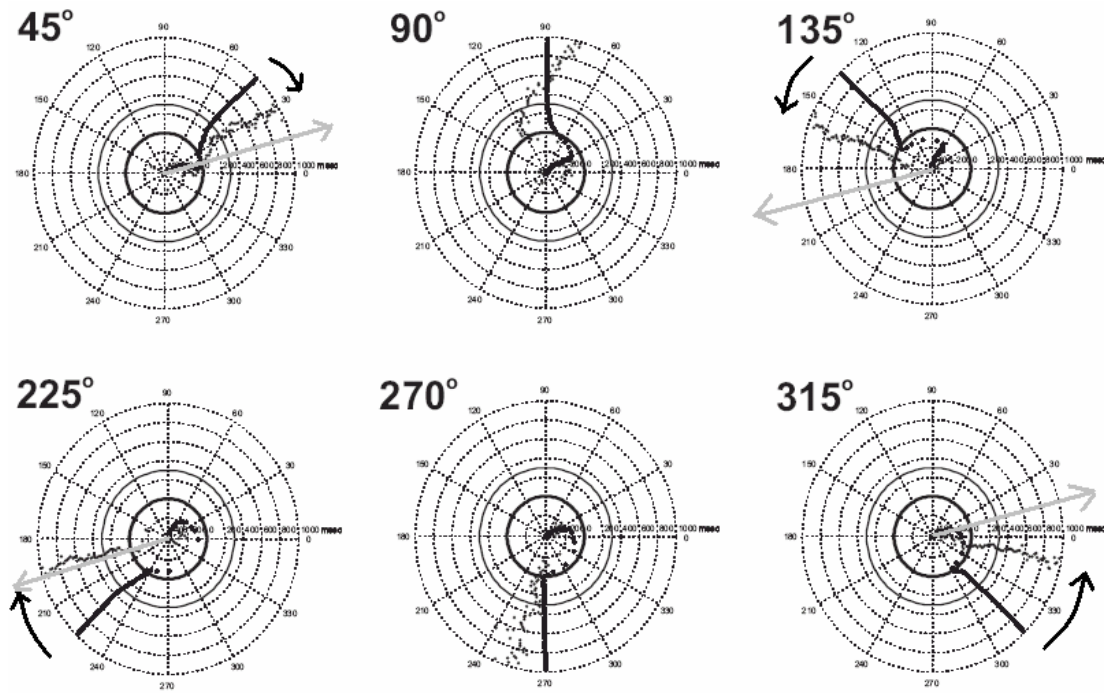
Figure 3: Direction-time trajectories of neuronal population vectors (solid line) and mean force output vectors (circles) for the 45°, 90°, 135°, 225°, 270°, and 315° force directions in the isometric task. All 132 neurons were used. This figure is based on Fig. 11 in [8] with permission. We've added arrows that show the direction in which the population vector deviates from the force direction (dark arrows). According to Supplementary Data 3 the PDs of the shoulder flexor and extensor are 14° and 194° respectively (gray arrows). In the 45° task the population vector deviates clockwise towards 14°. In the 135° task the population vector deviates counter-clockwise towards 194°,while in the of 225° task the population vector deviates clockwise towards 194°. In the 315° task the population vector deviates counter-clockwise towards 14°. In the 90° and 270° tasks the situation is less clear, as these directions are approximately in the middle between 14° and 194°.

Movement Task

Task description

Both the movement task and isometric task were part of the same experiment [8,20]. A particularly interesting aspect of the experiment is that the activity of the *same* neurons was recorded for the two different tasks (isometric and movement), enabling a detailed study of the (considerable!) change of activity of the same cell between tasks.

In the movement task the monkey was required to push a load in one of eight directions, spaced at 45º intervals. For a detailed description of the experimental setup see Supplementary Data 4.

Control Signal

A major prediction of our model pertains to the MCS. In Supplementary Data 4 we present the control signals predicted by our model, as well as explanations of how these results were derived. Similarly to the isometric task, we've used the predicted control signals in order to approximate the averaged response. Fig. 4 presents a comparison of the experimental results with the model prediction. In order

to reduce the effects of simple averaging procedure described in the legend of Fig. 4, we also compare the predicted control signal with a response of a *single* representative neuron in Fig. 5. As can be seen in Fig. 4 and 5, the temporal behavior of the neural signal predicted by the model corresponds to the experimental results. Particularly important is the fact that the results for both the isometric and the movement tasks reproduce the qualitative shift in neural activity between the two tasks.

a

b
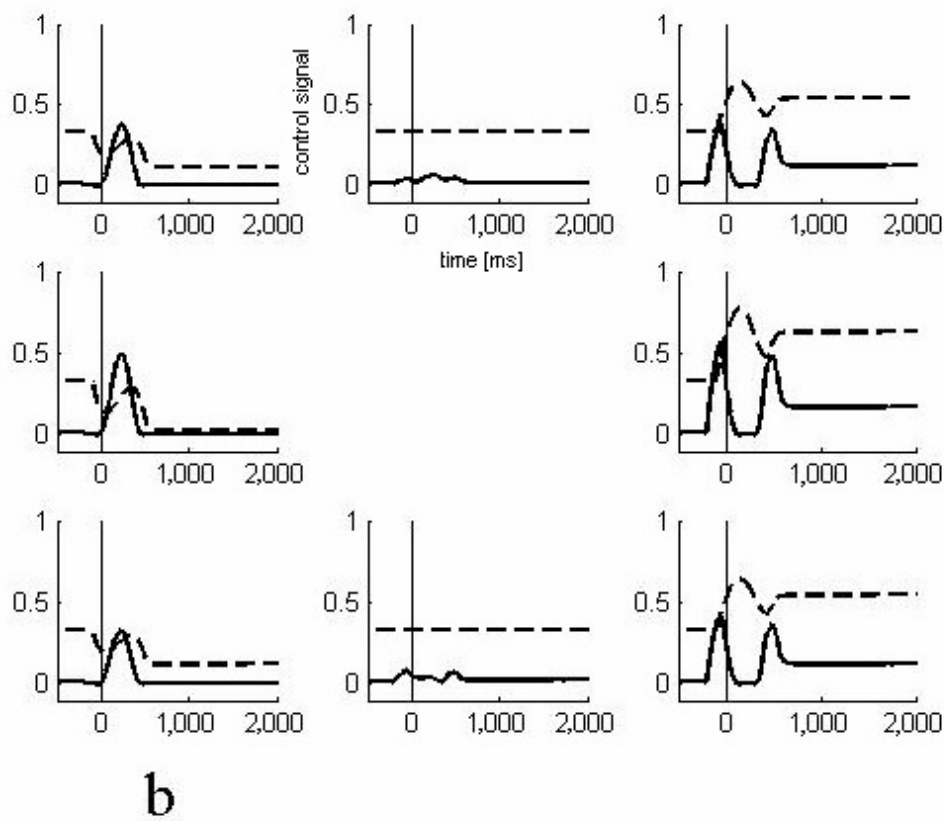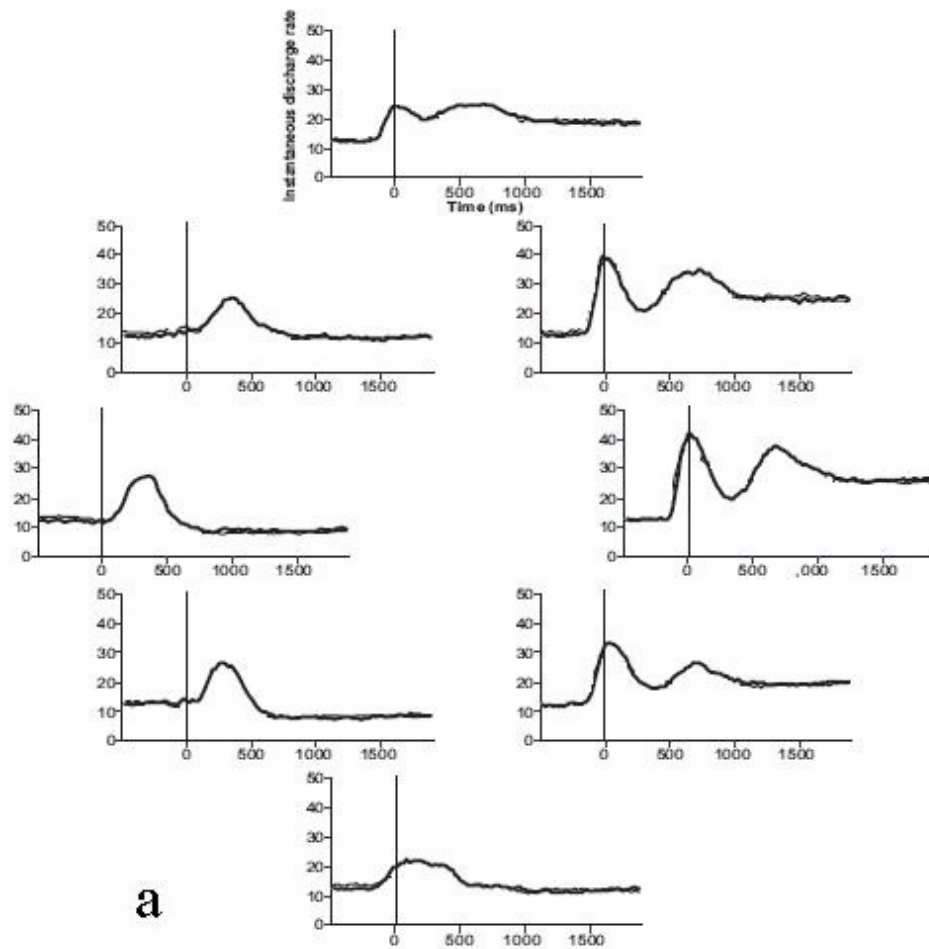
Figure 4: Population activity in the movement task. **4a:** Experiment, based on Fig. 9 of [8] with permission. Mean population response as a function of time and force direction, where the direction is relative to the PD of each cell. All data were aligned to the time of force onset (time 0) and the PD of each neuron, calculated at target hold time, was arbitrarily rotated to the right. **4b:** Simulation of shoulder extensor control signal in our model (solid line) and the control signal of TOD2000 (dashed line). The baseline and the normalization of the control signal of TOD200 are as in Fig. 1. We assume for both models that the control signal is delayed by 100msec. The ordinate of simulation of our control signal is normalized to the same arbitrary units as in Fig. 1b. The simulation of the averaged neural response was performed as in Fig. 1.
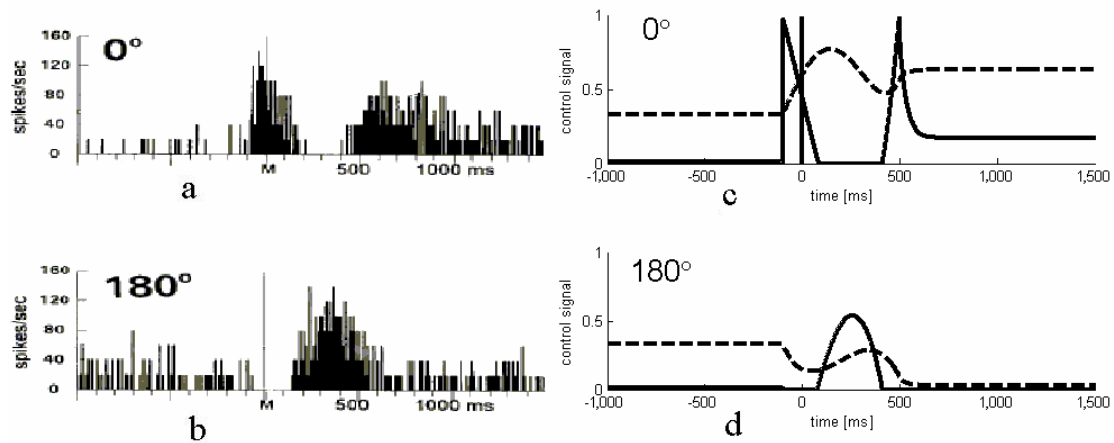
Figure 5: Movement task – comparison with activity of a representative cell. **5a:** Experiment, based on Fig. 1b from [20], with permission. Discharge pattern at the PD of a shoulder-related M1 cell in histogram format (10-ms bins). Data are aligned on the first significant force change, denoted by a solid vertical line (M). **5b:** The same as 5a, in the opposite direction. **5c:** Simulation of Shoulder extensor control signal in our model (solid line) and the control of TOD2000 (dashed line) at PD. The baseline and the normalization of the control signal of TOD200 are as in Fig. 1. We assume for both models that the control signal is delayed by 100msec. The ordinate of simulation of our control signal is normalized to arbitrary units.). **5d:** The same as 5c, in the opposite direction.

Single cell properties

There is no exact correspondence between the control signal and the single cell profile. However, the similarity is significant, as 56% of the cells displayed the burst-pause-burst response in their PD as shown in Fig. 5a. Most of these cells, as well as part of the cells in the remaining group, displayed a response of pause-burst-pause in the opposite direction as shown in Fig. 5b.

Cosine Tuning

The cosine function provided a good approximation to the temporal tuning function of the predicted control signal during most of the task period. The support of the predicted tuning function during most of the task period is about 180°. A detailed description of these results and an explanation of how they were derived are given in Supplementary Data 4.

The cosine tuning demonstrates again the similarity of the reported cosine tuning at the level of the single neuron to the predicted control signal.

We also expect that the support of a single neuron should be about 180° or less. This prediction is in agreement with the experimental results [8,20] shown in Supplementary Data 8. However, we do not have data about the tuning function support of all cells; such data is needed in order to further test this prediction.

Preferred Direction

Unlike the isometric task, the PD goes through a significant shift during movement. During each of two short periods, the PD changes by 180°. Consequently, there is a significant intermediate period, during which the PD is opposite to its 'normal' direction. Such behavior occurs also at the level of the single cell as shown in Fig. 6. Note that the PD goes through two reversals during the movement task.

Non Cosine Behavior

During the two short transition periods at which the PD is reversed, there are significant changes in the behavior of the tuning function. At these times the tuning function of the control signal is no longer similar to a cosine function, and its support deviates significantly from its value during the rest of the task. Such behavior occurs also at the level of the single cell as shown in Fig. 6. During the transition periods, cell activity was not directionally tuned (time windows represented by circles).

A prediction of our model (which needs to be tested experimentally) is that a non-cosine temporal tuning function and significant changes in the tuning function support occur during longer periods as the load become lighter. Detailed explanations of the above results are given in Supplementary Data 4.
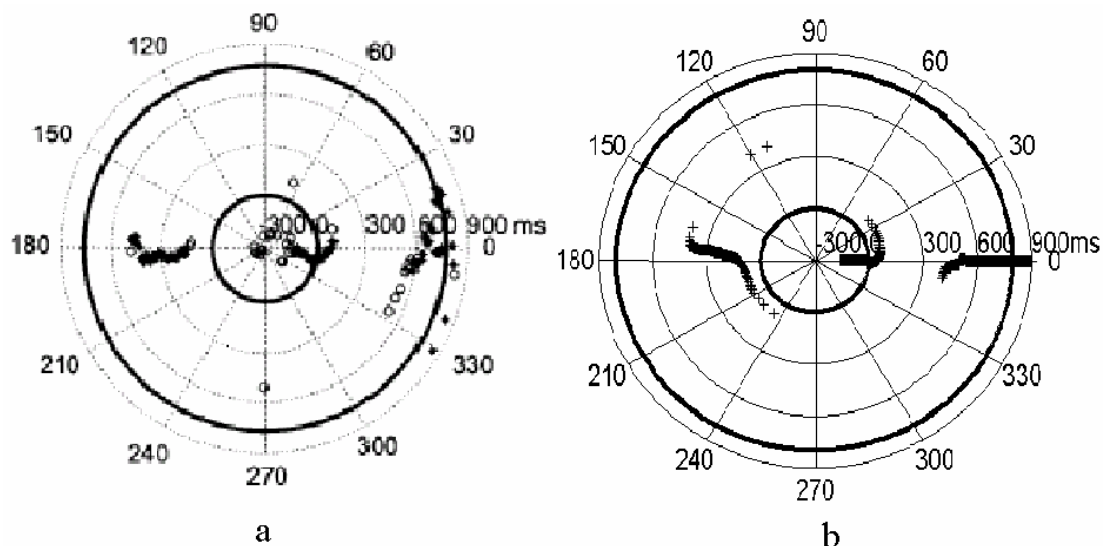
Figure 6: Reversals of the PD during movement task. **6a**: Based on Fig. 2b of [20], with permission. The temporal trajectory of the PD of a representative cell during movement tasks. The trajectory was determined by a 50ms sliding-window analysis. Time windows within which the cell was significantly related to direction are shown by an asterisk. Time windows within which the cell was not directionally related are shown by circle. Notice that during transition times (characterized by reversal of PD) the cell was *not* directionally tuned. Large thick concentric circles denote movement onset and offset. **6b** Simulation of shoulder extensor PD in our model. The PD was calculated as the angle at which the tuning function attains its maximum. The PD is relative to its value during target hold time.

Hand Location Dependence of Directional Tuning

The third experiment considered [19,23] examined the activity of M1 cells during a task, in which a monkey uses its arm to exert isometric forces at the hand, while the hand is held in one of nine different spatial locations on a plane. The major finding was that the discharge rate of all the recorded cells was significantly affected by the position of the hand. For a detailed description of the experimental setup see Supplementary Data 5.

We've calculated the PDs of muscle control signals (see Supplementary Data 5 for further details). Thus we were able to compare the location dependence of the control signal PD with the location dependence of a representative neuron in Fig. 7. The agreement between changes of the control signal PD based on the model (presented by arrows) and changes of the cell's PD in the experiment is clear. These results again establish the similarity between cell activity and the control signal activity, which explains the changes in the PD.
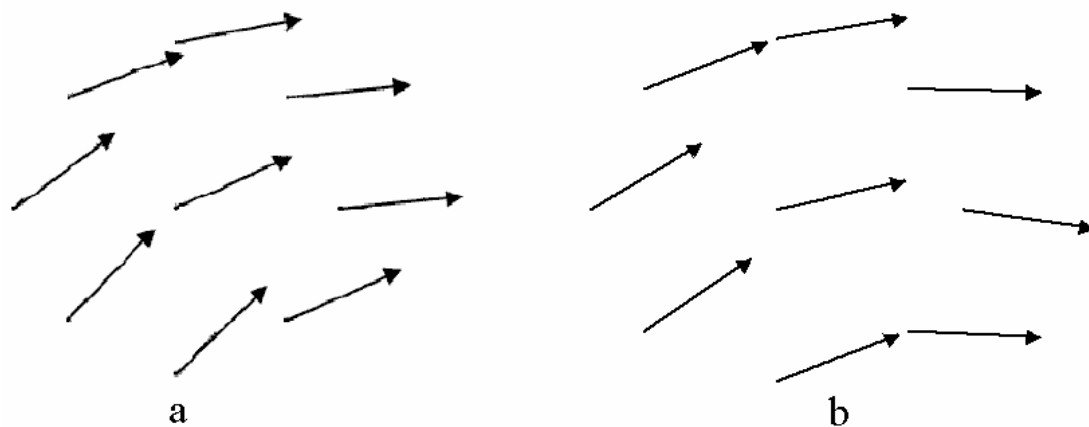
Figure 7: PD changes due to different hand locations. **7a:** Based on Fig. 1b of [19], with permission. Polar plot representation of the response of a single neuron at all 9 hand locations. The position of each arrow corresponds to the relative location of the hand on the planar work surface, with top arrow corresponding to most distal hand location. The arrow represents the PD with respect to the isometric force. **7b:** The same plot format displaying the prediction for the PDs of the shoulder flexor MCS according to our model.

Discussion

We have presented a system level physiological model for the generation of the control signal in primary motor cortex during certain voluntary tasks, based on combining optimal control ideas and bio-mechanical arm modeling. While we have been able to demonstrate good agreement with experimental results, many open questions remain for future research, of which we mention a few.

Relation to Prosthetic Controllers

Cortical neural prostheses are based on three components: microelectrodes and recording electronics, extraction algorithms and actuators [32]. The population vector [12,13,14] was the first extraction algorithm proposed. Since then, several advances in extraction algorithms were introduced e.g. the use of a generalized linear estimator [33], the use of dynamic estimation [34] and the use of dynamic kernels [35], to name but a few. Nevertheless, all the existing algorithms are purely 'black box' statistical algorithms. As far as we are aware, none of the current extraction algorithms use physiological models and parameters related to the internal mechanisms between neural control and end point movement. We believe that such extraction algorithm may be advantageous.

Movement in 3-D space

Our current model assumes 2-D tasks performed by a planar arm and a known hand trajectory. In order to generalize the model, further MCSs should be added, arm mechanics should include additional degrees of freedom of the shoulder joint and the influence of gravity should be taken into account.

More Accurate Models

Our model was aimed at being the simplest physiological model providing an explanation of basic properties of M1 neural activity. There is a well known trade-off between the accuracy of a model and its usefulness. This situation is typical to modeling of complex biological systems, as described by [36]: "In this section, a mathematical model of the growing embryo will be described. This model will be a simplification and an idealization, and consequently a falsification. It is to be hoped that the features retained for discussion are those of greatest importance in the present state of knowledge." Clearly there is room for more complex and accurate models.

One approach to achieving improved accuracy is using a more detailed model, which takes into account the dynamics of the spinal cord and all anatomical muscles along with their musculoskeletal geometry. Such an approach leads to many difficulties. In particular, we do not know how the spinal cord affects the system dynamics or how the effort is divided between more than 20 anatomical muscles surrounding the elbow and the shoulder. The computational complexity also increases with the number of muscles, since it increases the number of dimensions of the optimal control problem. Muscle models, which are relatively realistic[37,38,39] are dependent on several parameters and further parameters

are needed to describe musculoskeletal geometry. Estimating muscles and musculoskeletal geometry parameters is not a simple problem, especially in vivo [40].

A second approach is based on retaining the current level of abstraction, but replacing some of the model's components with more accurate equations. For example, it is known that muscle dynamics, musculoskeletal geometry and spinal cord feedback are influenced by joint angles and angular velocities. Though the combined influence of all these factors is unknown, we expect that joint angles and angular velocities have some influence on the neural control signal, beyond their indirect influence through arm mechanics. Therefore, in a more accurate model, Equation 2 of Methods may include the influence of joint angles and angular velocity.

Neural activity at the single cell level and neural network models

Our study shows that single cell behavior is *not* a mere manifestation of the properties of the muscle control signals. Consequently, our current model is limited in its ability to explain neural activity at the level of the single cell. We believe that some of the properties of single cell activity are a reflection of the architecture, dynamics and constraints imposed by the neural network, within which it is embedded. Therefore, in order to better understand the neural activity at the level of the single cell, our model should be extended by adding to it a neural network model, taking into account the major anatomical and physiological properties of the motor cortex. In particular, such a model is needed in order to extend our understanding towards representations of higher levels of control in the motor cortex. Finally, we should note that the problem of decoding the neural activity in the motor cortex is not separate from the issues of motor planning and learning.

Methods

The simplified model we propose consists of a transformation from the activity of M1 cells, through the muscle control signals, to joint torques and down to arm mechanics. In addition, we use an explicit optimization criterion in order to remove the inherent redundancy.

We consider a voluntary movement task, implying that the control signal is initiated from the motor cortex. The arm is assumed to be planar and gravity is neglected since all motion takes place in a horizontal plane. The joint redundancy is eliminated due to the one-to-one correspondence between hand position and the arm's joint angles in a horizontal plane. Moreover, we consider simple trained tasks, implying that we may assume the control signal is reproducible to a reasonable degree of accuracy, and that the control signal is optimized for the task in the sense of minimal co-contraction. The overall model non-linearity is a result of the separation between two antagonistic muscles as well as the multi-joint arm mechanics.

We proceed with a more detailed description of the model.

From neural activities to muscle control signals

The spinal cord is known to possess a rather complex functionality, especially in reflexive and rhythmic movements [2]. However, in the present context a model of the spinal cord, in which the MCS is simply a linear function of delayed neural inputs, has been presented and tested [21]. We have used this model while assuming four equivalent muscles: shoulder flexor, shoulder extensor, elbow flexor and elbow extensor. Specifically,

$$(1) \quad u_i(t) = \sum_j c_{i,j} n_j(t - d_{i,j})$$

where $u_i(t)$ is the control signal corresponding to the i-th muscle, $i = 1, \cdots, 4$, and $n_j(t)$ is the control signal corresponding to the j-th neuron, $j = 1, \cdots, N$.

In spite of Equation 1, the experimental results we've examined [8], show that the spinal cord takes part in the dynamic transformation of the control signal. For example, in the isometric task the neural response consisted of a pulse step while the EMG response consisted only of a step. See also section 6 of supplementary material concerning the contribution of the spinal cord to system dynamic. In our model the dynamic effect of the spinal cord, muscle dynamics and musculoskeletal geometry are all modeled together in a single unit as described in the following section.

From muscles control signals to joint torques

We have chosen a simple phenomenological model, in which the dynamic effect of the spinal cord, muscle dynamics and musculoskeletal geometry are all modeled together as a single unit. There are several motivations for this choice. Our model captures the essential low pass filter properties of the spinal cord and muscles using a single parameter which can be easily estimated from the data. Moreover, in the context of the modular multi-stage model we propose, there is a clear preference for simple components. Finally, this model seems to lead to satisfactory results in the context of the simple tasks considered. In spite the above, we plan to consider in the future the development of more complex but accurate models, as elaborated in the Discussion.

We have used the following equations to describe the connections between the MCSs $u_i(t)$ and the joint torques $\tau_i(t)$.

$$(2) \quad u_i(t) = \tau_i(t) + \alpha \frac{d\tau_i(t)}{dt}$$

$$(3) \quad \tau_{jo}(t) = \tau_{fl}(t) - \tau_{ex}(t) \quad \left(\text{jo-joint, fl-flexor, ex-extensor}\right)$$

The value of α was estimated to be 200 msec, leading to a good fit with experimental results.

Arm mechanics

We consider a standard bi-joint planar arm – see Fig. 8. The following transformations and relations can be found in standard Robotics textbooks (e.g. [41]).
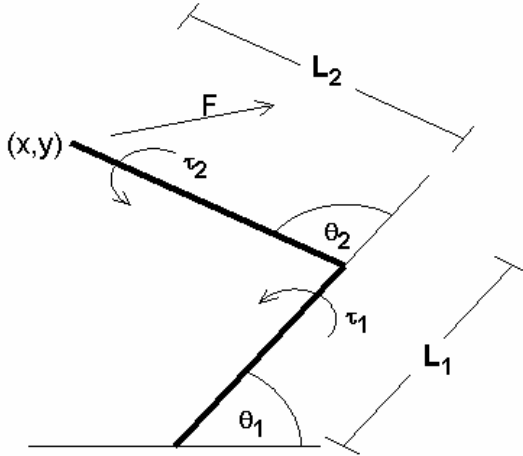
Figure 8: Arm Mechanic. L_1 and L_2 are upper arm and forearm lengths respectively. θ_1 and θ_2 are shoulder and elbow angles respectively. τ_1 and τ_2 are shoulder and elbow angles respectively. (x,y) are hand coordinates. F is the force vector exerted by the hand.

Kinematics
The transformation between joints angles and end-point coordinates is given by

$$(4) \quad x = L_1 \cos(\theta_1) + L_2 \cos(\theta_1 + \theta_2)$$
$$y = L_1 \sin(\theta_1) + L_2 \sin(\theta_1 + \theta_2)$$

Statics

The transformation between end-point force and joint moments is given by

(5) $\quad \underline{\tau} = J^T \underline{F}$

Where

$$J = \begin{bmatrix} -L_1\sin(\theta_1) - L_2\sin(\theta_1+\theta_2) & -L_2\sin(\theta_1+\theta_2) \\ L_1\cos(\theta_1) + L_2\cos(\theta_1+\theta_2) & L_2\cos(\theta_1+\theta_2) \end{bmatrix}$$

Dynamics

Denote by m_i the mass of link i, by r_i the distance between the joint and the center of link i and by I_i the inertia of link i. The relation between torques and movement is given by

(6) $\quad \tau_1 = H_{11}\ddot{\theta}_1 + H_{12}\ddot{\theta}_2 - h\dot{\theta}_2^2 - 2h\dot{\theta}_1\dot{\theta}_2$

$\quad\quad \tau_2 = H_{22}\ddot{\theta}_2 + H_{12}\ddot{\theta}_1 + h\dot{\theta}_1^2$

where

$H_{11} = m_1 r_1^2 + I_1 + m_2[L_1^2 + r_2^2 + 2L_1 r_2 \cos(\theta_2)] + I_2$

$H_{22} = m_2 r_2^2 + I_2$

$H_{12} = m_2 L_1 r_2 \cos(\theta_2) + m_2 r_2^2 + I_2$

$h = m_2 L_1 r_2 \sin(\theta_2)$

We have used the following values from [29,30,31]

$M_1 = 0.29 kg \quad\quad M_2 = 0.25 kg$

$L_1 = 14.4 cm \quad\quad L_2 = 15.4 cm$

$I_1 = 2.2\cdot10^{-4} kg\cdot m^2 \quad I_2 = 6.7\cdot10^{-4} kg\cdot m^2$

Optimization Criterion

The mechanism by which the brain selects a particular control signal leading to muscle activation and hand movement is not clear. Moreover, the huge redundancy in the system (at the level of trajectory selection, timing, joint-angle configurations and muscle activations) implies the need for some optimization based redundancy removing mechanism (see reviews in [42,43]). In general, there is no golden rule for the selection of such an optimization principle, and the utility of a particular principle rests on its biological plausibility and on the quality of its predictions. In the present context our task is somewhat simpler, since we assume complete knowledge of the trajectory. Moreover, because we assume a simple two-joint planar arm, there is no redundancy at the arm level.

Nevertheless, assuming a known trajectory and planar motion does not remove all redundancy, since the task can be achieved by many combinations of muscle activities. A redundancy exists even in the four muscle model we are considering, since co-contraction of antagonist muscles leaves room for many solutions. In order to resolve this redundancy, we have used an optimization criterion consisting of the sum of flexor and extensor MCSs, given by

$$(7) \quad P = \int_{t_0}^{t_f} [u_{fl}(t) + u_{ex}(t)]dt$$

where t_0 and t_f are the initial and final trajectory times, $u_{fl}(t)$ and $u_{ex}(t)$ correspond to the MCSs relating to the flexor and extensor respectively. In our simplified model, this criterion can be shown to be equivalent to the minimum torque co-contraction, as proved in Supplementary Data 1. Biologically, this criterion reflects the energy consumption of the muscles and of the neural networks, which control them.

References

[1] Dum R.P. & Strick P.L Motor areas in the frontal lobe: the anatomical substrate for the central control of movement. In: *Motor Cortex in Voluntary Movements*, edited by Riehle A. and Vaadia E. CRC Press, London 1–48 (2005).

[2] Kandel, E.R., Schwartz, J.H. & Jessel, T.M. *Principles of Neural Science*. McGraw-Hill, fourth edition (2001).

[3] Ashe, J. What Is Coded in the Primary Motor Cortex? In: *Motor Cortex in Voluntary Movements*, edited by Riehle A. and Vaadia E. CRC Press, London 1–48 (2005).

[4] Carmena, J.M. et al. Learning to Control a Brain-Machine Interface for Reaching and Grasping by Primates. *PLoS Biology*, **1(2)**, 1-16 (2003).

[5] Alexander, G.E. & Crutcher, M.D. Preparation for Movement: Neural Representations of Intended Direction in Three Motor Areas of the Monkey. *J Neurophysiology*, **64**, 133-150 (1990).

[6] Crutcher, M.D. & Alexander, G.E. Movement-Related Neuronal Activity Selectively Coding Either Direction or Muscle Pattern in Three Motor Areas of the Monkey. *J Neurophysiology*, **64**, 151-163 (1990).

[7] Kakei, S., Hoffman, D.S. & Strick, P.L. Muscle and movement representations in the primary motor cortex. *Science*, **285(5436)**, 2136–2139 (1999).

[8] Sergio, L.E., Hamel-Pêquet, C. & Kalaska, J.F. Motor cortex neural correlates of output kinematics and kinetics during isometric-force and arm-reaching tasks. *J Neurophysiology*, **94**, 2353-2378 (2005).

[9] Bernstein, N. *The Co-ordination and Regulation of MOVEMENTS*. Pergamon Press, London (1967).

[10] Georgopoulos, A.P., Kalaska, J.F., Caminiti, R. & Massey, J.T. On the relation between the direction of two-dimensional arm movements and cell discharge in primate motor cortex. *The Journal of Neuroscience*, **11**, 1527–1537 (1982).

[11] Georgopoulos, A.P., Kalaska, J.F. & Massey, J. Spatial coding of movements: A hypothesis concerning the coding of movement direction by motor cortical populations. *Experimental Brain Research (Supp.)*, **7**, 327–336 (1983).

[12] Georgopoulos, A.P., Schwartz, A.B. & Kettner, R.E. Neuronal population coding of movement direction. *Science*, **233**, 1357-440 (1986).

[13] Schwartz, A.B., Kettner, R.E. & Georgopoulos, A.P. Primate motor cortex and free arm movements to visual targets in three-dimensional space. I. Relations between single cell discharge and direction of movement. *J. Neurosci.*, **8**, 2913-27 (1988).

[14] Georgopoulos, A.P., Kettner, R.E., Schwartz, A.B. Primate motor cortex and free arm movements to visual targets in three-dimensional space. II. Coding of the direction of movement by a neuronal population. *J. Neurosci.*, **8**, 2928-37 (1988).

[15] Johnson, M., Mason, C. & Ebner, T. Central processes for the multiparametric control of arm movements in primates. *Current Opinion in Neurobiology*, **2(11)**, 684–688 (2001).

[16] Scott, S.H. & Kalaska, J.F. Changes in Motor Cortex Activity During Reaching Movements With Similar Hand Paths But Different Arm Postures. *J Neurophysiological*, **73**, 25632567 (1995).

[17] Scott, S.H. & Kalaska, J.F. Reaching Movements With Similar Hand Paths But Different Arm Orientations. I. Activity of Individual Cells in Motor Cortex. *J Neurophysiological*, **77**, 826–852 (1997).

[18] Scott, S.H., Gribble P.L., Graham K.M. & Cabel D.W. Dissociation between hand motion and population vectors from neural activity in motor cortex.

[19] Sergio, L.E. & Kalaska, J.F. Systematic changes in directional tuning of motor cortex cell activity with hand location in the workspace during generation of static isometric forces in constant spatial directions. *J Neurophysiological*, **78**, 1170–1174 (1997).

[20] Sergio, L.E. & Kalaska, J.F. Changes in the temporal pattern of primarymotor cortex activity in a directional isometric force versus limb movement task. *J Neurophysiological*, **80**, 577–1583 (1998).

[21] Morrow, M.M. & Miller, L.E. Prediction of muscle activity by populations of sequentially recorded primary motor cortex neurons. *J. Neurophysiology*, **89(4)**, 2279–2288 (2003).

[22] Feldman, A.G., Adamovitch, S.V., Ostry, D.J. & Flanagan, J.R. The origin of electromyograms-explanations based on the equilibrium point hypothesis. In: *Multiple Muscle Systems. Biomechanics and Movement Organization*, edited by Winters JM and Woo SL-Y. New York: Springer-Verlag 195–213 (1990).

[23] Sergio, L.E. & Kalaska, J.F. Systematic Changes in Motor Cortex Cell Activity With Arm Posture During Directional Isometric Force Generation. *J. Neurophysiol.*, **89**, 212–228 (2003).

[24] Mussa-Ivaldi F.A. Do neurons in the motor cortex encode movement direction? an alternative hypothesis. *Neuroscience Letters*, **91**, 106–111 (1988).

[25] Todorov, E. Direct cortical control of muscle activation in voluntary arm movements: a model. *Nature Neuroscience*, **3**, 391–398 (2000).

[26] Todorov, E. On the role of primary motor cortex in arm movement control. *In Progress in Motor Control*, **III, 6**, 125–166 (2002).

[27] Moran, D.W. & Schwartz, A.B. Letters to the editor. *Nature Neuroscience* **3(10)**, 963 (2000).

[28] Amirikian, B. & Georgopoulos, A.P. Motor cortex: coding and decoding of directional operations. In: *Handbook of Brain Theory and Neural Networks*, edited by Arbib, M. MIT Press, second edition 452 (2001).

[29] Cheng, E.J. & Scott, S. H. Morphometry of macaca mulatta forelimb. I shoulder and elbow muscles and segment inertial parameters. *J. Morphology.*, **245**, 206–224 (2000).

[30] Melis E. H., Richmond, F.J.R., Singh, K. & Scott, S.H. Morphometry of macaca mulatta forelimb. II fiber-type composition in shoulder and elbow muscles. *J. Morphology.*, **251**, 323– 332 (2002).

[31] Graham, K.M. & Scott, S. H. Morphometry of macaca mulatta forelimb. III moment arm of shoulder and elbow muscles. *J. Morphology.*, **255**, 301–314 (2003).

[32] Schwartz, A. B. Cortical Neural Prosthetics. *Annu. Rev. Neurosci.*, **27**, 487-507 (2004).

[33] Salinas. E. & Abbott L.F. Vector reconstruction from firing rates. *J. Comput. Neurosci.,* **1**, 89-107 (1994).

[34] Wu, W. et al. Modeling and Decoding Motor Cortical Activity Using a Switching Kalman Filter. *IEEE Transactions on Biomedical Engineering,* **51**, 6 (2004).

[35] Shpigelman, L. Singer Y., Paz R. & E Vaadia. Spikernels: Predicting Arm Movements by Embedding Population Spike Rate Patterns in Inner-Product Spaces. *Neural. Computation.*, **17**, 671–690 (2005).

[36] Turing, A. M. *The Chemical Basis of Morphogenesis, Phil Trans Royal Soc London B*, **237**, 37—72 (1952).

[37] Zajac, F.E. Muscle and tendon: Properties, models, scaling, and application to biomechanics and motor control. *Crit Rev. Biomed. Eng.*, **17**, 359–411 (1989).

[38] Winters J. M. & Stark L. Analysis of Fundamental Human Movement Patterns Through the Use of In-Depth Antagonistic Muscle Models. *IEEE Transactions on biomedical engineering*, **32**, **10**, 826-839 (1985).

[39] Cheng E.J., Brown I.E. & Loeb G.E. Virtual muscle: a computational approach to understanding the effects of muscle properties on motor control. *Journal of Neuroscience Methods*, **101**, 117-130 (2000).

[40] Garner B.A. & Pandy M.G. Estimation of Musculotendon Properties in the Human Upper Limb. *Annals of Biomedical Engineering*, **31**, 207-220 (2003).

[41] Asada H. & Slotine J.J.E. *Robot Analysis and Control*. Wiley Interscience (2000).

[42] Engelbrecht S. Minimum principles in potor control. *J. Math. Psychol.*, **45(3)**, 497–542 (2001).

[43] Pandy M.G. Computer modeling and simulation of human movement. *Annu. Rev. Biomed. Eng.*, **3**, 245–73 (2001). 366.

[44] Flash T. & Hogan N. The Coordination of Arm Movements: An Experimentally Confirmed Mathematical Model. *The Journal of Neuroscience*, **5(7)**, 1688-1703 (1985).

Supplementary Information

1. Optimization Criteria Equivalence

From Equations (2) and (3) in Methods, repeated here for ease of reference,

$$u_i(t) = \tau_i(t) + \alpha \frac{d\tau_i(t)}{dt} \quad \alpha > 0,$$

$$\tau_{jo}(t) = \tau_{fl}(t) - \tau_{ex}(t) \quad jo - \text{joint}, \quad fl - \text{flexor}, \quad ex - \text{extensor},$$

we find that

$$(1) \quad u_{fl}(t) - u_{ex}(t) = \tau_{jo}(t) + \alpha \frac{d\tau_{jo}(t)}{dt}.$$

From Supplementary Equation 1, it is easy to see that the control functions $u_{(fl)}^o(t), u_{(ex)}^o(t)$, which

minimize the objective function $\int_{t_0}^{t_f} [u_{(fl)}(t) + u_{(ex)}(t)]dt$ (Equation 7 in Methods), under the

constraint $u_i(t) \geq 0$ for all t are given by:

$$(2) \quad u_{fl}(t) = \left[\tau_{jo}(t) + \alpha \frac{d\tau_{jo}(t)}{dt} \right]_+ ,$$

$$u_{ex}(t) = \left[-\left(\tau_{jo}(t) + \alpha \frac{d\tau_{jo}(t)}{dt} \right) \right]_+ .$$

Any other solution $u_{fl}(t), u_{ex}(t)$ increases both control signals at some point during the task.

Now, from $u_i(t) = \tau_i(t) + \alpha \frac{d\tau_i(t)}{dt}, \quad \tau_i(0) = 0$, we get that

$$(3) \quad \tau_i(t) = \frac{e^{-\frac{t}{\alpha}}}{\alpha} \int_0^t u_i(s) e^{\frac{s}{\alpha}} ds .$$

Therefore, for any other solution $u_{fl}(t), u_{ex}(t)$, in which both MCSs are increased at some point

during the task, both torques are also increased at least at one point. Therefore, $u_{fl}^o(t), u_{ex}^o(t)$ also

minimize the objective function given by

$$(4) \quad P = \int_{t_0}^{t_f} [\tau_{fl}(t) + \tau_{ex}(t)]dt ,$$

where $\tau_{fl}(t)$ and $\tau_{ex}(t)$ correspond to the torques produced by the flexor and extensor muscles,

respectively.

2. TOD2000

The Model

The model[25,26], to which we refer as TOD2000, is based on two equations. Supplementary Equation 5 describes the population activity,

$$(5) \quad U \cdot c(t-d) = F^{-1} \cdot f_{ext}(t) + m \cdot \ddot{x}(t) + b \cdot \dot{x}(t) + k \cdot x(t)$$

Let us denote the number of neurons by N. The matrix U (of dimension $2 \times N$) contains the 2D PDs of the neurons. The vector c (of dimension $N \times 1$) contains the temporal firing rates of the neurons, and the delay d is constant. The vector f_{ext} (of dimension 2×1) is the external endpoint force. The vector $x(t)$ (of dimension 2×1) is the endpoint position.

The matrix $F^{-1} = \begin{bmatrix} \dfrac{\sqrt{2}}{2} & 0 \\ 0 & \sqrt{2} \end{bmatrix}$, and the parameter values are m = 1kg, b = 10 Ns/m, k = 50 N/m.

Supplementary Equation 6 describes the single cell activity,

$$(6) \quad c_j(t-d) = \overline{c}_j + \frac{u_j^T}{2}\left(F^{-1}f_{ext}(t) + m_j\ddot{x}(t) + k_j x(t)\right) + b_j\left[u_j^T\dot{x}(t)\right]_+,$$

where $\overline{c}_j, m_j, k_j, b_j$ are specific neuronal parameters chosen from independent uniform distributions $U[0; 2\overline{c}]$, $U[0; 2m]$, $U[0; 2b]$ and $U[0; 2k]$ respectively. The vector u_j^T (of dimension 1x2) is a unit vector pointing in the PD of neuron i.

The Non-Physiological Nature of TOD2000

TOD2000 was presented as a physiological model. However, Supplementary Equations 5 and 6 show that this model is based on non-physiological assumptions.

1) The population vector is used as a basic assumption of TOD2000 (l.h.s. of Supplementary Equation 5). The population vector of course *assumes* direction coding rather than constituting a physiological assumption.

2) Each of the two components of the produced control signal is characterized independently by an equation of a point mass on a spring (r.h.s. of Supplementary Equation 5). While this pair of independent equations may have some mechanical interpretation, this interpretation has nothing to do with bi-joint arm mechanics. Recall that the basic properties of the arm mechanics are: (a) The influence of each joint on both external coordinates (Equations 4 and 5 in Methods); (b) The mutual dynamic influence between the two joints (Equation 6 in Methods). Furthermore, the control signal of TOD2000 (r.h.s. of Supplementary Equation 5) ignores the antagonistic muscles as well. As we show in this study, antagonistic muscles are

24

basic physiological ingredients of the system and are essential for understanding the neural activity in M1.

3) In TOD2000, both directionality and cosine tuning are imposed in a way which has nothing to do with arm biomechanics (the multiplication by u_j^T in Supplementary Equation 6).

4) The distribution of the neural activities (the use of $\overline{c}_j, m_j, k_j, b_j$ in Supplementary Equation 6 is a further non-physiological assumption of TOD2000.

Comparison with the Experimental Results

While our model is aimed at explaining neural activity in a specific area of M1, Todorov[25,26] does not distinguish between different areas of M1, which is assumed to be homogeneous. However, in [26] the isometric and movement experiments [20] we have examined, are explicitly cited as being in agreement with his model. Unfortunately we have not been able to reproduce this purported agreement when using TOD2000.

1) In the isometric task (Fig. 1 and 2 in Results) TOD2000 does not predict the overshoot. The model predicts a symmetric change between the response at the PD and the response at the opposite direction, while the experimental results show that the change of neural activity at the PD is significantly larger.

2) In the movement task (Fig. 4 and 5 in Results) there seems to be little similarity between TOD2000 and the experimental data. For example, in graph 5c corresponding to 0° one observes a single wide burst instead of the burst-pause-burst pattern.

3) In Supplementary Equation 6 of TOD2000 a very high diversity in the neural activity of cells is assumed in a non physiological fashion. This description is at odds with experimental results, in which a small number of typical behaviors were observed, rather than a huge continuum of behaviors. Another curiosity is that the above suggested distribution sometimes leads to negative firing rates.

4) According to TOD2000 cosine tuning has nothing to do with arm mechanics and is accounted for only by noise minimization. The cosine tuning is imposed in a non physiological fashion and the predicted support is always 360°. This basic assumption and prediction of TOD2000 is clearly at odds with at least some experimental result showing 180° support. The periods of non-cosine behavior during movement task are also not explained by TOD2000.

5) In TOD2000 the PD is constant. The changes in PD during the movement task (Fig. 6 in Results), and the differences in the PDs through different hand locations (Fig. 7 in Results) cannot be explained.

6) The model of TOD2000 assumed a population vector scheme as one of the model's non physiological basic assumptions. Consequently, the population vector direction is expected in this model to always be identical with force direction. The observed deviations of the population vector from the force direction (Fig. 3 in Results) cannot be explained by such a model.

3. Isometric Task

Task Description

In the first experiment[8,20], a juvenile rhesus monkey (a.k.a. Macaca mulatta) was trained to perform an isometric task, i.e. the monkey retained a fixed end-point position in the face of an external force field. The monkey held a static handle exerting a 0.3N force away from its body during 1-3 seconds (center hold time). Then the monkey was required to exert a ramp force of 1.5N in one of eight directions. Force directions were spaced at 45° intervals, starting at 0°. We've estimated the shape of the force ramp, according to graph 1A[20], as a second order spline with a rise duration of 200mSec. The handle was positioned in front of the monkey. The starting hand location was at the midline, 20cm in front of the sternum. We've estimated the position of the monkey's sternum to be 5cm away from its shoulder. Therefore, the right hand position in our simulation was (-5cm, 20cm) in shoulder coordinates corresponding to (55.8°, 92.5°) in joint coordinates. Whenever the monkeys performed the task with the left arm, all collected data were subjected[8] to a mirror-image transformation about the 90°-270° (Y) axis. Therefore, we've simulated only the right arm. The activity of single cells in the caudal part of M1 was recorded during the task. Most neurons were related to the shoulder and shoulder girdle, with a smaller number related to the elbow.

Predicted Tuning Function

First, we analyze the case of static force exertion in different directions.

The force, relative to a bias $\underline{F}_0$, is equal in all directions.

$$(7) \quad \underline{F} = \underline{F}_0 + F \begin{bmatrix} \cos(\varphi) \\ \sin(\varphi) \end{bmatrix}$$

The relation between end-point force and joint moments is given by Equation 5 in Methods i.e.,

$$\begin{bmatrix} -l_1 \sin(\theta_1) - l_2 \sin(\theta_1 + \theta_2) & l_1 \cos(\theta_1) + l_2 \cos(\theta_1 + \theta_2) \\ -l_2 \sin(\theta_1 + \theta_2) & l_2 \cos(\theta_1 + \theta_2) \end{bmatrix} \begin{bmatrix} F_{0x} + F \cos(\varphi) \\ F_{0y} + F \sin(\varphi) \end{bmatrix},$$

hence

$$(8) \quad \underline{\tau} = \begin{bmatrix} \tau_{01} + \tau_1 \cos(\varphi - \varphi_1) \\ \tau_{02} + \tau_2 \cos(\varphi - \varphi_2) \end{bmatrix},$$

where

$$\tau_{01} = \{-l_1 \sin(\theta_1) - l_2 \sin(\theta_1 + \theta_2)\} \cdot F_{0x} + \{l_1 \cos(\theta_1) + l_2 \cos(\theta_1 + \theta_2)\} \cdot F_{0y}$$

$$\tau_{02} = -l_2 \sin(\theta_1 + \theta_2) F_{0x} + l_2 \cos(\theta_1 + \theta_2) F_{0y}$$

$$\tau_1 = F\sqrt{l_1^2 + l_2^2 - 2l_1 l_2 \cos(\theta_2)}$$

$$\tau_2 = Fl_2$$

$$\varphi_1 = \tan^{-1}\left(\frac{l_1 \cos(\theta_1) + l_2 \cos(\theta_1 + \theta_2)}{-l_1 \sin(\theta_1) - l_2 \sin(\theta_1 + \theta_2)}\right) = \tan^{-1}\left(\frac{y}{x}\right) + \frac{\pi}{2} \quad \text{where } (x, y) \text{ are hand coordinates}$$

$$\varphi_2 = \theta_1 + \theta_2 - \frac{\pi}{2}.$$

Since the external force is constant, according to Equation 2 in Methods $u_i(t) = \tau_i(t)$, and thus

$$u_{sho-flexor} - u_{sho-flexor} = \tau_{01} + \tau_1 \cos(\varphi - \varphi_1)$$

$$u_{elb-flexor} - u_{elb-flexor} = \tau_{02} + \tau_2 \cos(\varphi - \varphi_2).$$

Due to Equation 7 in Methods, the torque production is divided between the flexor and the extensor control signal in such a way, that the flexor control signal produces the positive part of the cosine wave and the extensor control signal produces the negative part.

$$(9) \quad u_{sho-flexor} = \left[\tau_{01} + \tau_1 \cos(\varphi - \varphi_1)\right]_+$$

$$u_{sho-extensor} = \left[-\tau_{01} + \tau_1 \cos(\varphi - \varphi_1 - \pi)\right]_+$$

$$u_{elb-flexor} = \left[\tau_{02} + \tau_2 \cos(\varphi - \varphi_2)\right]_+$$

$$u_{elb-extensor} = \left[-\tau_{02} + \tau_2 \cos(\varphi - \varphi_2 - \pi)\right]_+.$$

Thus, the control signals are cosine tuned as shown in Supplementary Fig. 1.
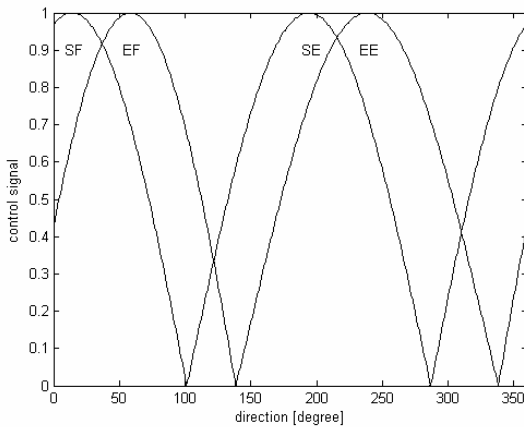
Supplementary Figure 1: Tuning functions of 4 control signals predicted by our model. SF, EF, SE and EE stand for shoulder flexor, elbow flexor, shoulder extensor and elbow extensor respectively. The tuning functions are normalized to [0, 1].

We present an intuitive explanation of the cosine tuning. Consider small movements of the elbow joint as displayed in Supplementary Fig. 2. In this case, the joint is free to move only in the directions 0° and 180°.
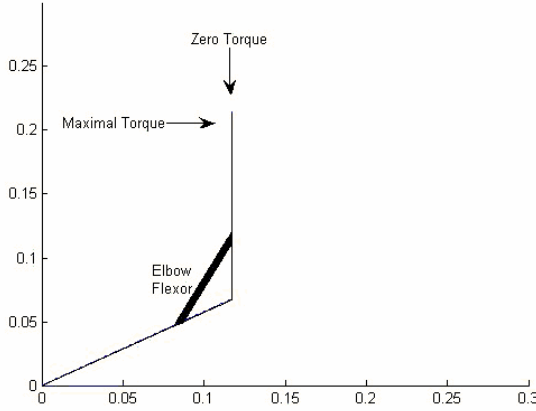
Supplementary Figure 2: Elbow flexor PD.

In order to keep the forearm static (as is required for the isometric task), the external force should be compensated for by an opposite force. In the example in Supplementary Fig. 2 the external force in direction 180° will elicit a force response by the elbow flexor. Similarly, an external force in the direction 0° will elicit a force response by the elbow extensor. On the other hand, an external force applied at either 90° or 270° will lead to a response by the rest of the body. Therefore, only the projection of the external force on the axis, in which the elbow joint is free to move, influences the elbow joint. Notice that axis direction depends on hand position and therefore, the elbow axis is not always 0°-180°. The support of each of the control signals (the range of directions in which the signal is not zero) depends on τ_{01} or τ_{02}. If $\tau_{01} = \tau_{02} = 0$ then the support of all 4 MCSs is 180°. In the experimental setup we've examined there was a small bias of external force. Therefore the support of each of the 4 MCSs is not exactly 180° as shown in Supplementary Table 1.

	Shoulder Flexor	Shoulder Extensor	Elbow Flexor	Elbow Extensor
PD	14°	194°	58°	238°
Support	175°	185°	160°	200°

Supplementary Table 1

Preferred Directions

The PD in the context of the isometric experiment is defined as the direction of external force at which the signal amplitude is maximal. According to Supplementary Equation (9) the PDs of the MCSs are:

$$
(10) \quad
\begin{aligned}
&\varphi_{sho-flexor} = \tan^{-1}\left(\frac{y}{x}\right) + \frac{\pi}{2} \quad \varphi_{sho-extensor} = \varphi_1 - \frac{\pi}{2} \\
&\varphi_{elb-flexor} = \theta_1 + \theta_2 - \frac{\pi}{2} \quad\quad \varphi_{elb-extensor} = \theta_1 + \theta_2 + \frac{\pi}{2}.
\end{aligned}
$$

The specific values for the experimental setup we've examined are given in Supplementary Table 1.

Predicted Control Signal

If the control signal in its PD were defined merely relative to the muscle torque, then we would get a signal with similar shape to the torque profile. However, the control signal is also related to the first derivative of the torque. Therefore, instead of getting a step response, we get a pulse step response.
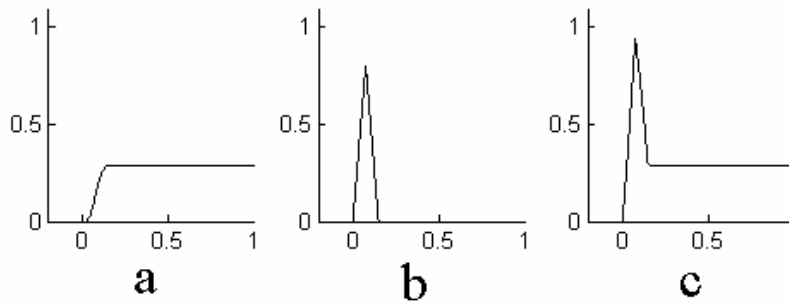
Supplementary Figure 3: Pulse step response in the isometric task. The units are arbitrary. **3a**: Step of muscle torque. **3b**: First derivative of Supplementary Fig. 3a. **3c**: Combined pulse step response.

In order to obtain the full spectrum of responses, the above profile is multiplied by the tuning function of the control signal as shown in Supplementary Fig. 4, which shows the response for one of the four control signals. The four control signals are similar, except for their PD. Since Fig. 4 is aligned to the PD of the control signal, we show the response of only one of the four control signals.
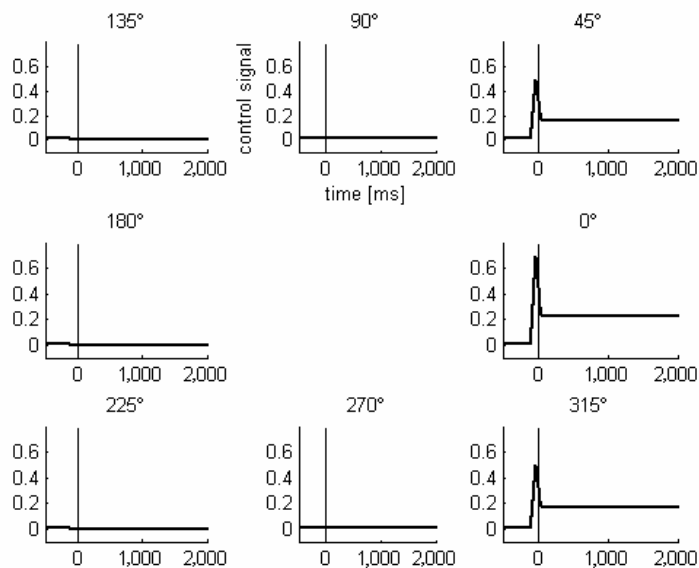
Supplementary Figure 4: Simulation of shoulder extensor control signal aligned to its PD. We assume here a delay of 100msec. The ordinate of the simulation is normalized to arbitrary units.

4. Movement Task

Task Description

In the movement task the monkey was required to push a load of 1.3kg by 8cm. Movement duration was about 0.6sec, and the directions of movement were spaced at 45° intervals, starting at 0°. Since we did not have experimental data about the hand trajectory in the movement task, we assumed a minimum jerk trajectory [44], i.e.

$$x(t) = x_0 + (x_0 - x_f)(15r^4 - 6r^5 - 10r^3)$$
$$y(t) = y_0 + (y_0 - y_f)(15r^4 - 6r^5 - 10r^3)$$

where $r = \dfrac{t}{t_f}$; x_0, y_0 *and* x_f, y_f *are hand coordinates at* $t = 0$ *and at* $t = t_f$ *respectively.*

Similarly to the isometric task, the monkey was required to initially exert a force of 0.3N away from its body. The inertial force during movement was calculated according to the relation $F = ma$. After movement the monkey was required to exert a force of about 1N against the pendulum. We've assumed that the force profile following the movement period is described by $F(t) = 1 - ae^{-bt}$, where *a and b* are chosen in a way that retains the continuity of the force and its first derivative at the end of movement.

Isometric Force Approximation

The predicted results for this task are more difficult to explain. In this non-linear case, we do not introduce exact analytical results, but rather provide an intuitive explanation. First, note that when the hand performs a minimum jerk trajectory, its acceleration is characterized by a wave profile shown in Supplementary Fig. 5.
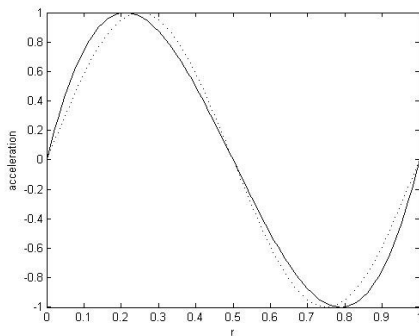
Supplementary Figure 5: Hand acceleration during a minimum jerk trajectory. Solid line: minimum jerk trajectory- $a(r) \propto 2r^3 - 3r^2 + r$ *where* $r = t/t_f$ (the units are arbitrary). Dotted line: the function- $\sin(2\pi t)$.

First we will use the following approximation. Let us assume an isometric force experiment, in which the force profile is given by $F(t) = m \cdot a(t)$ where m is the mass of the external load and $a(t)$ is described by a minimum jerk trajectory as shown in Supplementary Fig. 5. Under such simplified

30

assumptions we can calculate the joint torques in a similar way to the isometric task and find that the torque profile has the wave profile of Supplementary Fig. 5 multiplied by a cosine tuning function (Supplementary Fig. 6, thin line). We refer to this approximation as the *isometric force approximation*. There are two differences between this approximation and an accurate description of arm mechanics:

  (a) The tuning function is not constant since the PD changes during movement as joint angles change. In the experimental setup we've examined, this effect is relatively insignificant.

  (b) Besides moving the load, the muscles also need to move the arm itself. This effect is calculated using the dynamics (Equation 6 in Methods). In our experimental setup the mass of the load is relatively high and therefore this effect is also not significant.

Supplementary Fig. 6 shows the predicted joint torques in eight directions aligned to the flexor PD in the isometric task. The thick line shows the exact prediction and the thin line shows the isometric force approximation discussed above. It can be seen that the isometric force approximation is close to the real torque trajectory. In fact, this approximation can be even further improved if the mass of the load is increased a little in order to compensate for some part of the arm dynamics.
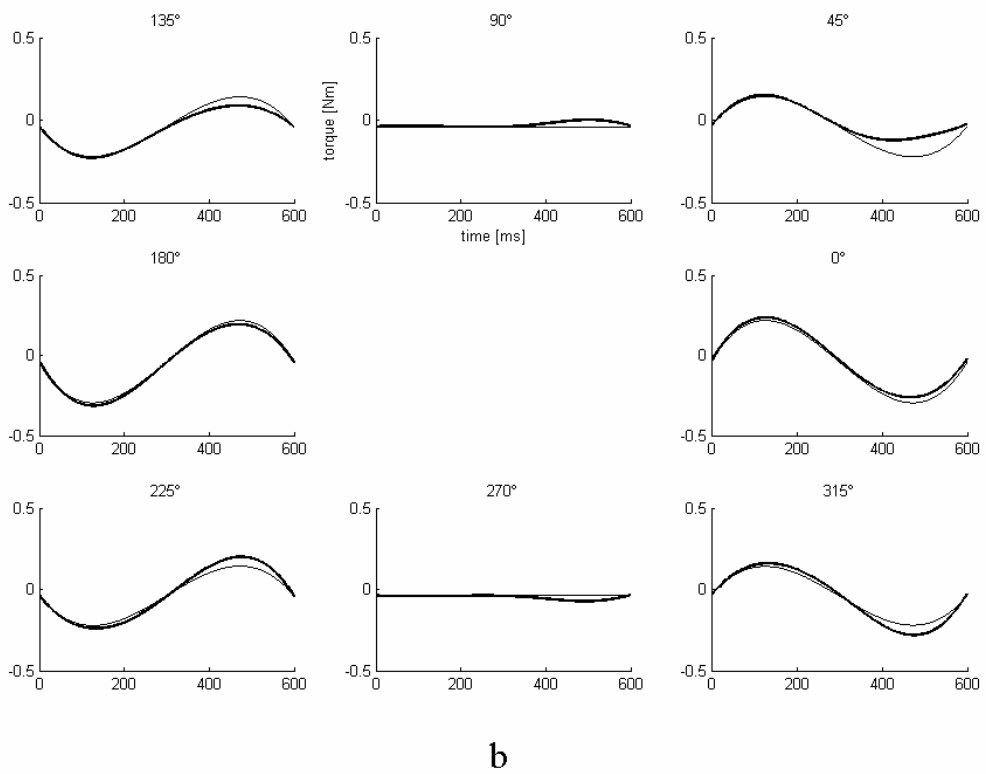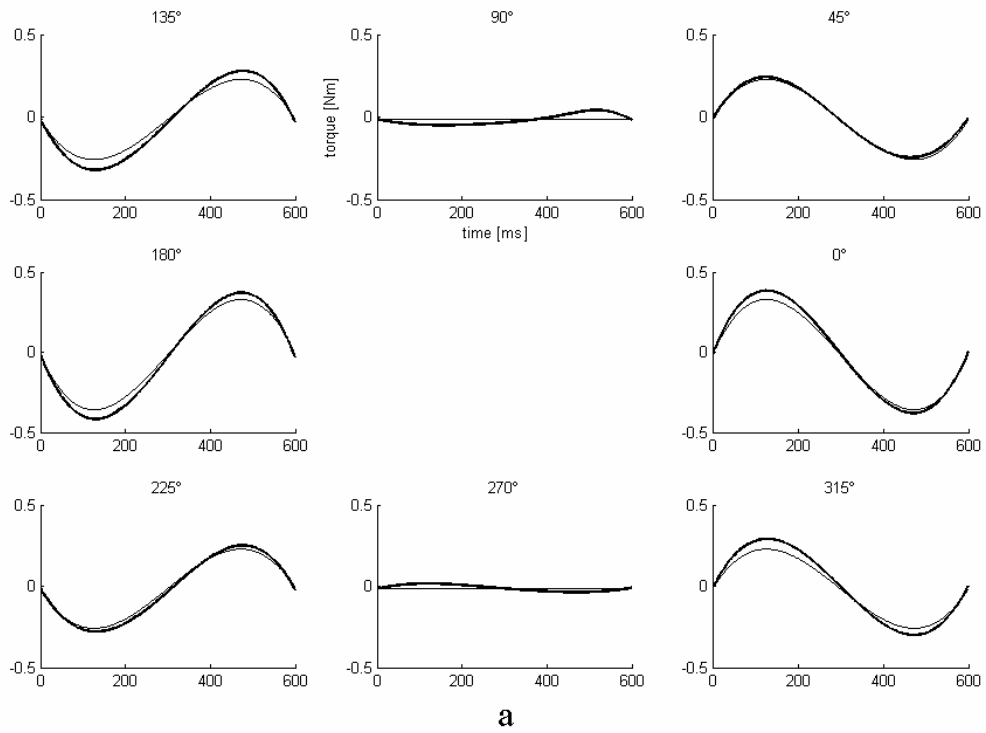
Supplementary Figure 6: Joint torques during the movement experiment. **2a:** Shoulder **2b:** Elbow.

Tuning function

Since the torque can be approximated using the isometric force approximation, it is approximately cosine tuned. Therefore, from Supplementary Equation 2 in Supplementary Data 1, it follows that MCSs are approximately cosine tuned as well. This conclusion is in agreement with simulation results – during most of the task, the tuning function is well approximated by a cosine function.

Supplementary Fig. 7 shows the support of the temporal tuning function during a movement task. During most of the task the support is about 180°, which agrees with our previous analysis.
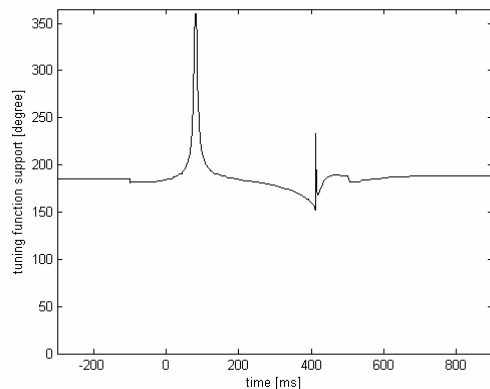
Supplementary Figure 7: Shoulder extensor control signal: Tuning function support.

A significant distortion of the support from its typical value occurs around two transition times (next section explains why we called them transition times). In fact, these unusual values are not the only unusual phenomenon at these periods. Close to the transition time the shape of the tuning becomes very different from cosine – see an example in Supplementary Fig. 8.

Our simulation shows that the phenomena of unusual support and lack of cosine tuning behavior become more apparent as the load becomes lighter. The reason for this is the non linear aspect of arm dynamics, which becomes more significant at small loads, where the isometric force approximation is poor.
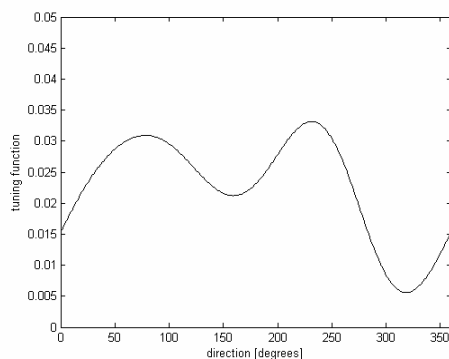
Supplementary Figure 8: Temporal tuning function in the movement task at time = 80 msec.

Predicted Control Signal

The resulting wave shaped torque is produced by two antagonistic muscles. If the neural signal were immediately converted into a torque we would obtain a bi-phasic response: one muscle would produce a burst during the first part of movement and the antagonistic muscle would produce a burst during the rest of the movement. However, due to the delayed response of the muscle (the component related to torque derivative in Equation 2 in Methods) things are more complex. Instead of a bi-phasic response we obtain a tri-phasic response: a burst of one control signal followed by a burst of the antagonistic control signal and again a burst of the first control signal. We refer to the transition times between the first phase and the second and between the second and third phases as transition times.

The tri-phasic response is better understood when we consider how torque is divided between the antagonistic muscles as shown in Supplementary Fig. 9. When the neural input to a muscle ceases, the torque does not vanish immediately, since it has some decay period. In order to change the torque rapidly enough, the antagonistic muscle should be activated, while the first muscle is still active.
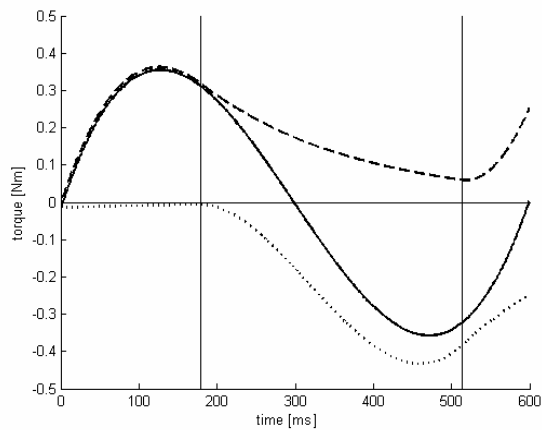
Supplementary Figure 9: Shoulder muscle torques in the movement task. Movement direction is 0. The dashed line is the flexor torque, the doted line is extensor torque and the solid line is the total shoulder torque. Vertical lines denote transitions between antagonist control signals.

The control signal results from the multiplication of the tri-phasic response with an approximate cosine tuning function as shown in Supplementary Fig. 10.

34
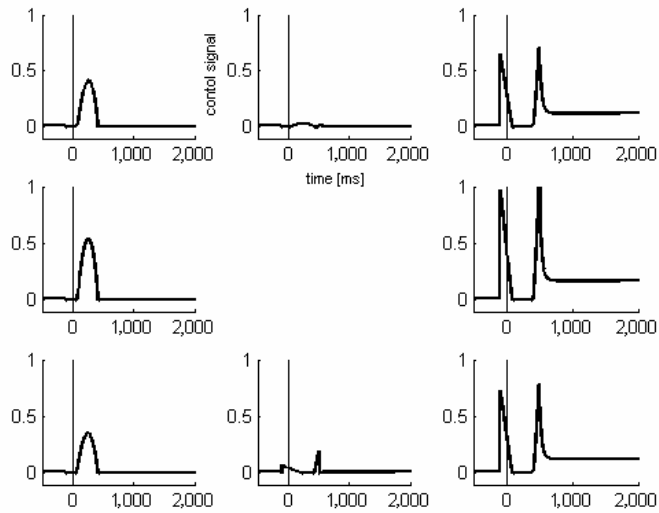
Supplementary Figure 10: Simulation of shoulder extensor control signal aligned to its PD. We assume here a delay of 100msec. The ordinate of the simulation is normalized to arbitrary units.

Unlike the isometric task, the total neural control to a joint, $u_{(fl)}(t) - u_{(ex)}(t)$, has three phases rather than one. It has a first positive (or negative) phase followed by a second negative (or positive) and then a third positive (or negative) phase. Therefore, during the second phase the PD is approximately opposite to the PD, characterizing the first and third phases. This is a basic and highly non-linear property of the system caused by the division of torques between two antagonistic muscles. Intuitively, it also helps to understand how the operation of the system looking at the spectrum of responses in Supplementary Fig. 10, while remembering that the response of the control signal in a certain direction is similar to the response of the antagonistic control signal at the opposite direction.

5. Hand Location Dependence of Directional Tuning

Task Description

The third experiment considered [19,23] examined the activity of M1 cells during a task, in which a monkey uses its arm to exert isometric forces at the hand, while the hand is held in one of nine different spatial locations on a plane. In the first location the conditions were similar to the isometric task examined at the beginning of the result section. The remaining 8 hand locations were at a distance of 8cm, spaced at 45º intervals, starting at 0º.

Predicted Preferred Direction of Control Signals

Using the Supplementary Equations 10 in Supplementary Data 3, we've calculated the PD of the MCSs shown in Supplementary Fig. 11.
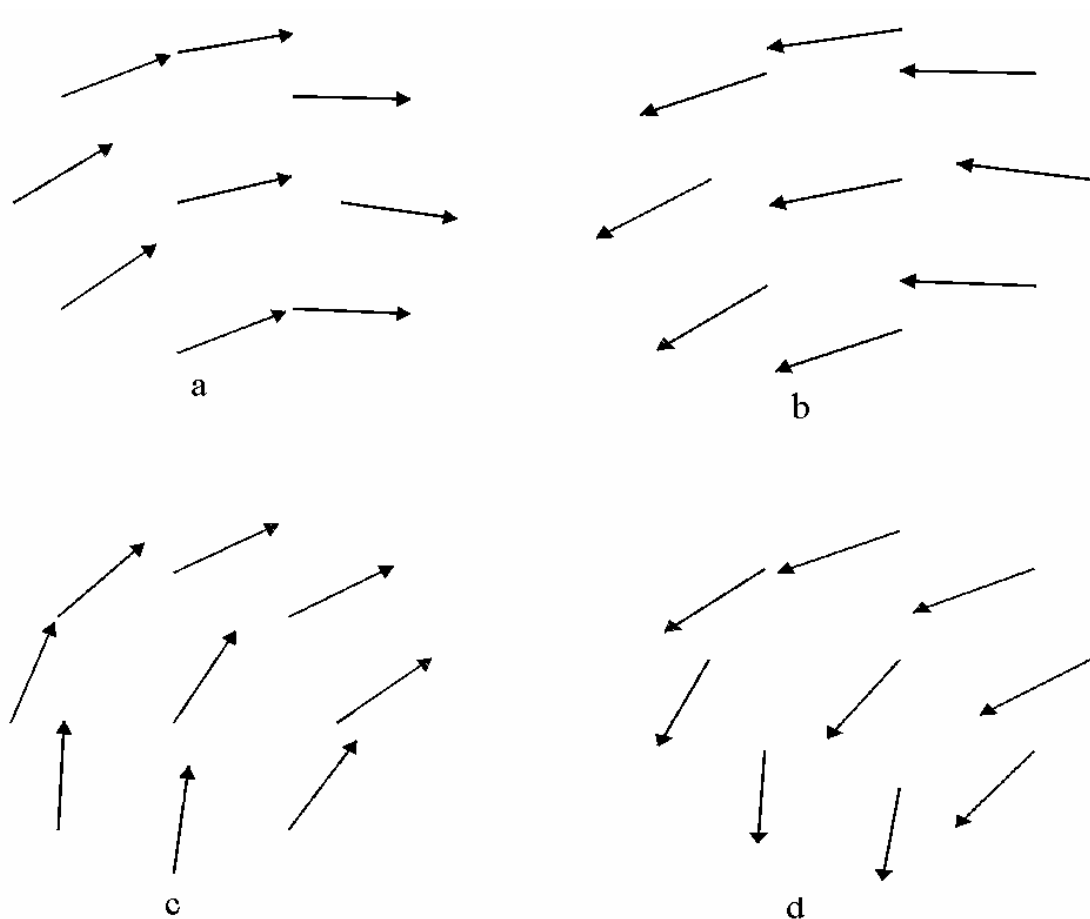
Supplementary Figure 11: PD changes due to different hand locations. Polar plot representation of the response of a single neuron at all 9 hand locations. The position of each arrow corresponds to the relative location of the hand on the planar work surface, with the top arrow corresponding to the most distal hand location. The arrow represents the PD with respect to the isometric force. **11a:** Shoulder flexor. **11b:** Shoulder extensor. **11c:** Elbow flexor. **11d:** Elbow extensor.

6. Sensitivity Analysis

Our simulation uses eight estimated parameters: upper arm mass, length and inertia; forearm mass, length and inertia; the distance of the monkey's sternum from its shoulder and the torque derivative coefficient. In this section we address the sensitivity of the results to model parameters.

Lengths and Hand Position

The value of the PD was not relevant to most results, as these were calculated relative to the PD. In muscle directionality amplification (Fig. 3 in Results) the values of the PD of the shoulder flexor and the shoulder extensor have been used. The PDs (Supplementary Equations 10 in Supplementary Data 3) depend on 3 estimated parameters: the upper arm length (L1), the forearm length (L2), and hand position (X0, Y0). Hand position was estimated, as we did not know the exact value of the distance of the monkey's sternum from its shoulder (-X0). Since the PD of each extensor is opposite to that of its antagonistic flexor, we examined only the flexor PDs. We've changed each of the relevant parameters over a wide range, while retaining the remaining parameters at their fixed estimated values. The results are shown in Supplementary Table 2.

-X0	**5cm**	3cm	8cm	5cm	5cm	5cm	5cm
L1	**14.4cm**	14.4cm	14.4cm	12cm	17cm	14.4cm	14.4cm
L2	**15.4cm**	15.4cm	15.4cm	15.4cm	15.4cm	12cm	20cm
Sho-fl	**14°**	9°	22°	14°	14°	14°	14°
Elb-fl	**58°**	54°	64°	49°	68°	57°	56°

Supplementary Table 2: The bold column is according to the estimated parameters we've used. Blank cells stand for values which are the same as our estimated values.

Supplementary Table 2 shows that the predicted PD of the shoulder flexor is in the range of 9°-22° over a reasonable range of parameters. Thus the result concerning muscle directionality amplification is robust.

Torque Derivative Coefficient

Supplementary Fig. 12 is similar to Fig. 2c in Results (prediction of shoulder extensor control signal in isometric task at PD), but here we show the results for different values of the torque derivative coefficient (α). The pulse-step response appears for all values of α. The value of α only determines the relative height of the pulse in the pulse-step response.
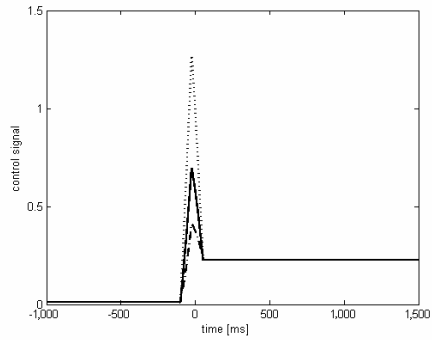
Supplementary Figure 12: Influence of α (torque derivative coefficient) value on the isometric task prediction. The shoulder extensor control signal at the PD. Dashdot line: α = 0.1. Solid line: α = 0.2. Dotted line: α = 0.4.

Supplementary Fig. 13 is similar to Fig. 5c in Results (prediction of shoulder extensor control signal in isometric task in the PD and in the opposite direction), but here we show the results for different values of α. The tri-phasic response appears for all values of α. The value of α only determines the following. Movement in the PD: the first pulse gets higher but narrower with the increase of α, while the second pulse gets higher but narrower with the increase of α. Movement in the opposite direction: the pulse shifts to the left and becomes higher with the increase of α.

a   b
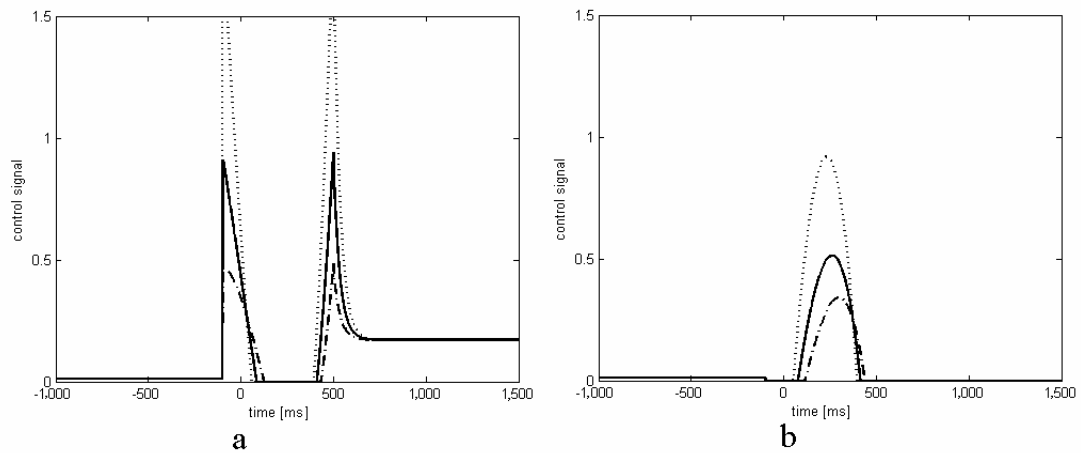
Supplementary Figure 13: Influence of α (torque derivative coefficient) value on the movement task prediction. The shoulder extensor control signal. Dashdot line: α = 0.1. Solid line: α = 0.2. Dotted line: α = 0.4. **13a**: Movement at the PD. **13b**: Movement in the opposite direction.

Interestingly, the changes of the response, due to increasing α, are similar to the reported changes between the EMG and the neural activity in M1[8]. This shows that beside the muscles, the spinal cord has a significant contribution to the overall low pass filter property of the system.

Even though our estimation of this parameter may be inexact (and can be improved, once we have more detailed experimental data) the pulse-step pattern in the isometric task and the three-phasic pattern in the movement task are robust.

Masses and Moments of Inertia

The masses ($M1$, $M2$) and the moments of inertia ($I1$, $I2$) influence arm dynamics (Equation 6 in Methods) only during the movement task. As we've shown in Supplementary Data 4, arm dynamics is not significant in the setup we've examined. Therefore, the influence of an inaccuracy in $M1$, $M2$, $I1$ and $I2$ is insignificant as well.

7. Muscle Directionality Amplification

Amplification of the PD θ_x implies that neurons with a PD which is close to θ_x are more dominant. Consequently, the population vectors are shifted towards θ_x. How may this happen? The response of a cosine tuned neuron may be represented by

$$(11) \quad f(\theta) = h \left[\frac{\cos(\theta - \theta_{PD}) - \cos(d/2)}{1 - \cos(d/2)} \right]_+ ,$$

where θ_{PD} is the PD, h is the peak height and d is the support of the tuning function.

The dominance of a certain direction θ_x may be achieved in two ways.

a) Relatively higher peaks (or equivalently higher density) of neurons with PD close to θ_x (Supplementary Fig. 14b).

b) Higher support of neurons with PD close to θ_x (Supplementary Fig. 14c).

Either way, the result is a shift of the population vector towards θ_x as shown in Supplementary Fig. 14.
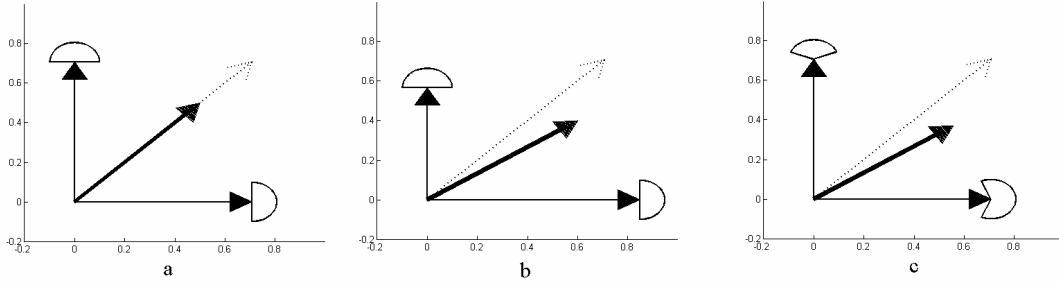
Supplementary Figure 14: Amplification of the 0° PD. The dotted arrow at 45° depicts force (or movement) direction. The solid thin arrows at 0° and 90° are neuronal PDs, where the size of the arrow represents the peak height of the tuning function and the arc at the end of the arrow represents the support of the tuning function. The thick arrow represents the population vector. Units are arbitrary. **14a:** The peak heights and the supports of the two neurons are equal and the direction of the population vector is identical to the force direction. **14b:** The peak height of the tuning function of the 0°-neuron is higher than the peak height of the tuning function of the 90°-neuron. Consequently, the population vector shifts towards 0°. **14c:** The support of the tuning function of the 0°-neuron is wider than the support of the tuning function of the 90°-neuron. Consequently, the population vector shifts towards 0°.

8. Tuning Function Support in the Level of the Single Cell

Our model consists of 4 equivalent muscles. This enables a neuron to influence more than a single equivalent muscle. In fact, such cases certainly occur, as the arm contains several double-joint anatomical muscles. Double joint muscles (also known as bi-articular muscles) are muscles surrounding two joints and serving as extensor or flexor for both. Whether a neuron influences more than a single equivalent muscle through neural network connectivity or through bi-joint anatomical muscles, such situation needs to be further analyzed.

Supplementary Data 3 shows a large range of directions (136°), over which flexor control signals of different joints are active together. The overlap of extensor control signals of the two joints is similar. In general, an overlap between flexors (or extensors) of 90°-180° exists for all reaching ranges of the arm. This is a result of arm geometry. Since $L1 \cong L2$ the difference δ between the PDs of the flexors is one of two equal angles in a triangular. See in Supplementary Fig. 15.
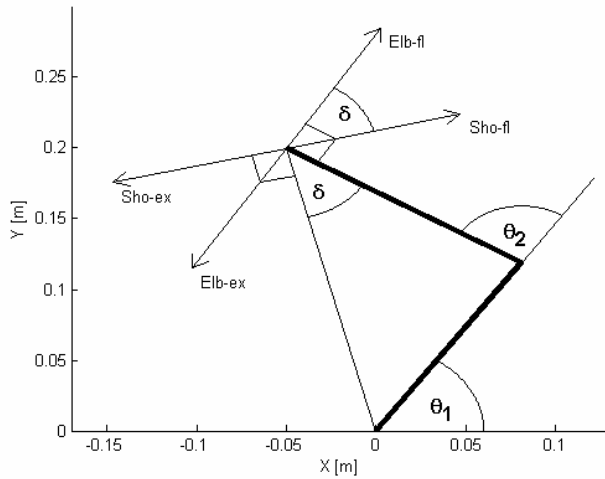
Supplementary Figure 15: Preferred Directions. Upper arm length, forearm length and hand position are the same as the setup in the isometric task. The arm is denoted by a bold line. θ_1 and θ_2 are shoulder angle and elbow angle respectively. PDs are denoted by arrows, where 'Sho' stands for shoulder, 'Elb' stands for Elbow, 'fl' stands for flexor and 'ex' stands for extensor. The angle δ is the difference between the PDs of the flexors (or extensors).

Therefore, the overlap between flexors (or extensors) is $90^0 \leq (180^0 - \delta) \leq 180^0$ and the overlap between flexors and extensors of different joints is $0^0 \leq \delta \leq 90^0$ for all the reaching ranges of the arm. The overlap between the flexor and the extensor of the same joint is always 0^0. Since neurons are known to possess broad tuning functions, we expect that neurons influence more than a single muscle, especially in the case of two flexors or two extensors, where a large overlap of activity regions exists.

In summary, the support of the tuning function is expected to be about 180° in the case of neuronal influence on a single (equivalent) muscle and about 135° (on average) in the case of influence on two muscles. We do not have the experimental data needed to test this prediction for all neurons. However,

Supplementary Fig. 16 and Supplementary Fig. 17 show examples of a representative neuron in both tasks, where the support is about 180°.
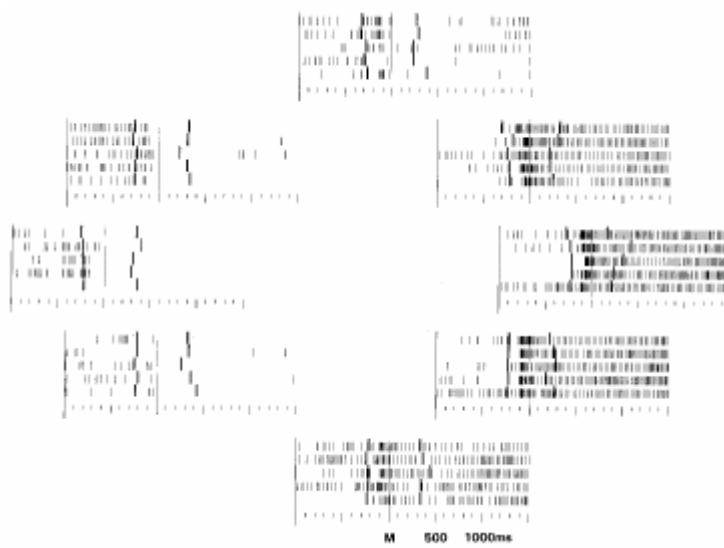
Supplementary Figure 16: Cell directional response in isometric task, based on Fig. 1a[20] with permission. Discharge pattern of a shoulder-related M1 cell during the isometric force task. Each raster illustrates cell activity during 5 trials, and raster location corresponds to the direction of the force. Data are aligned on the 1st significant force change, denoted by a solid vertical line (M). For each trial, the heavy tick mark to the left of the cursor movement onset line shows the time of target onset and the heavy tick mark to the right shows the time at which the final static level of force within the peripheral target was attained. It can be seen that after the force change (M) the response is about zero at four out of eight directions. Therefore, the tuning function support is about 180°.
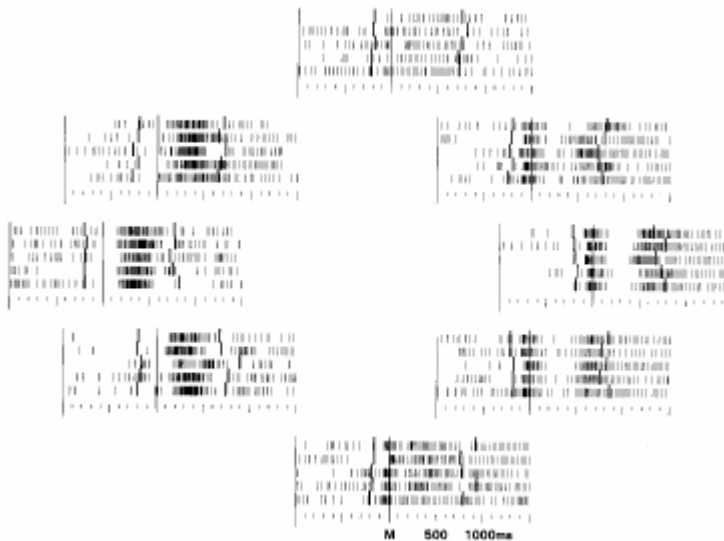
Supplementary Figure 17: Cell directional response in the movement task, based on Fig. 1b[20] with permission. Discharge pattern of a shoulder-related M1 cell during the movement task. Each raster illustrates cell activity during 5 trials, and raster location corresponds to the direction of movement. Data are aligned on movement initiation, denoted by a solid vertical line (M). For each trial, the heavy tick mark to the left of the cursor movement onset line shows the time of target onset and the heavy tick mark to the right shows the time at which the final static level of force within the peripheral target was attained. It can be seen that the support is about 180°. For example, out of eight directions, four display zero response at time = 0, while the remaining four directions display non-zero response at time = 0.

42